UNIVERSITY OF CAPE COAST

DETECTIONOF TRACE GAS (WATER VAPOUR) USING QUANTUM

CASCADE LASER OPEN - PATH SYSTEM (QCLOPS) VERSION 2

SENSOR AND THE ANALYSIS OF SMOKE FROM SOME SELECTED

WOOD SPECIES

CHARLES LLOYD YEBOAH AMUAH

2011

UNIVERSITY OF CAPE COAST

DETECTIONOF TRACE GAS (WATER VAPOUR) USING QUANTUM

CASCADE LASER OPEN - PATH SYSTEM (QCLOPS) VERSION 2

SENSOR AND THE ANALYSIS OF SMOKE FROM SOME SELECTED

WOOD SPECIES

BY

CHARLES LLOYD YEBOAH AMUAH

THESIS SUBMITTED TO THE DEPARTMENT OF PHYSICS, SCHOOL

OF PHYSICAL SCIENCES, UNIVERSITY OF CAPE COAST, IN

PARTIAL FULFILMENT OF THE REQUIREMENTS FOR AWARD OF

MASTER OF PHILOSOPHY DEGREE IN PHYSICS

JUNE 2011

DECLARATION

Candidate's Declaration

I hereby declare that this is the result of my own original research and that no part of this has been presented for another degree in this university or elsewhere.

……………………………….   Date……………………..

Charles Lloyd YeboahAmuah

(Candidate)

Supervisors' Declaration

We hereby declare that the preparation and presentation of the thesis we supervised were in accordance with the guidelines on supervision of thesis laid down by the University of Cape Coast.

……………………………….   Date…………………………

Dr. Moses Jojo Eghan

(Principal supervisor)

……………………………….   Date…………………………

Prof. Claire F. Gmachl

(Co-supervisor)

ABSTRACT

A Quantum Cascade Laser Open-Path System (QCLOPS) version 2 sensor has been set-up and used to measure water vapour in the troposphere. The QCLOPS version 2 sensor was compared with a commercial humidity sensor. A positive correlation of 71.46 % was established between the coefficient of variation of the version 2 sensor and the mass concentration of the commercial humidity sensor.

Ten different wood species namely Kroma, Dwindwinaba, Esia,Yaya, Konkroma, Emire, Mango, Esakoko, Cocoa and Aborday were studied to ascertain the chemical compounds emitted during combustion. Volatile organic compounds (VOCs) such as Acetone, Acrolein, 2-Butanone and Benzene were found in these wood species with gas concentrations ranging between 65.2898 - 20.6254, 131.9121 - 9.4528, 20.6529 - 5.6554 and 1.8760 - 0.3982 respectively. Semi-volatile organic compounds (SVOCs) such as Benzyl alcohol and 2-Methylphenol were also found in these wood species with gas concentrations ranging between 119.7127 - 10.9159 and 5.3206 - 0.2796 ppm respectively.

Finally, direct absorption method and Fourier Transform Infrared (FT-IR) Spectrometer were used to measure Benzyl alcohol and 2- Methylphenol in the laboratory. The infrared absorption spectra of Benzyl alcohol and 2-Methylphenol showed absorption at 1020, 1036, 1080 and 1108, 1176 cm^{-1} respectively. This compares well with the Know-it-All infra-red database. The results show the capability of a future sensor to measure these gases in the field.

ACKNOWLEDGEMENTS

forgetting all the staff members of the Department. I greatly cherish their part they played in my training here in this Department and am really grateful.

Finally, l would like to acknowledge my family members and friends for the love and support they shared with me during this period of work.

DEDICATION

This thesis is dedicated to my late father Mr John KwekuAmuah, my mother

AbenaaPomaa and my sisters Mrs Alicia Naykene and Adriana Rene Amuah

and my uncle Yaw NtowAbabio.

TABLE OF CONTENTS

Content   **Page**

LIST OF TABLES

LIST OF FIGURES

LIST OF PLATES

CHAPTER ONE

INTRODUTION

In recent years, climate change issues, especially the greenhouse effect, have taken the centre stage in everyday discussions throughout the world. This is as a result of the effects it is having on our survival. Trace gases that occur naturally are water vapour, carbon dioxide, methane, nitrous oxide and ozone. The ones that result exclusively from human industrial activities are hydrofluorocarbons (HFCs), perofluorocarbons (PFCs) and sulphur hexafluorocarbons (SF_6). These trace gases contribute to the greenhouse effect.

These gases are also called greenhouse gases and are mostly found in the troposphere. These gases absorb some of the heat from outer space and trap it near the earth's surface thereby warming the earth surface. The amount of heat trapped by these greenhouse gases determines the temperatures on the surface of the earth.

Water vapour accounts for about 90 % of all greenhouse gases. The remaining 10 % is due to carbon dioxide, methane, nitrous oxide and others. Water vapour is extremely important in considering weather and climate issues. It accounts for the existence of clouds, rain or snow. It evaporates from the surface of the earth and eventually returns as precipitation-rain or snow. When water evaporates to form water vapour, heat is absorbed(Water Vapour Confirmed as Major Player in Climate Change, n.d.) thereby leading to the

cooling of the earth. An increase in water vapour will result only when another greenhouse gas carbon dioxide is increased (Water Vapour Confirmed as Major Player in Climate Change, n.d.). The temperature increases when carbon dioxide traps more heat from outer space (Water Vapour Confirmed as Major Player in Climate Change, n.d.). This results in more water vapour being evaporated from the surface of the earth.

Increase in carbon dioxide results from the burning of solid waste, fossil fuels (oil, natural gas and coal) and volcanic eruptions. Forest burning also produces a lot of carbon dioxide. In Ghana, several wood species are used as a fuel in cooking, baking bread and preservation of fish (by smoking). These wood species when burnt release harmful gases such as Acetone, Acrolein, 2-Butanone, Benzene, Benzyl alcohol, 2-Methylphenol and others. According to the Center for Disease Control and Prevention (2011), human exposure to these gases can have damaging effects. Some of the short term effects of these gases are that they may causeirritation of the eyes and respiratory tract. They affect the central nervous system, liver, kidney and possibly gastrointestinal tract. Prolonged exposure can have effects on the blood and the bone marrow. They can cause lung oedema and may also result in unconsciousness. Benzene for instance is considered to be carcinogenic to humans (Center for Disease Control and Prevention (2011); United States Department of Labour, n.d.; Wikipedia, 2011; American Cancer Society, 2010; U. S. Environmental Protection Agency, 2011). There is therefore the need for monitoring these gases for effective control.

There are several methods used for measuring the concentration of water vapour. The conventional method is the use of hygrometers. Optical

methods such as Differential Optical Absorption Spectroscopy (DOAS), Differential Absorption Light detection and ranging (DIAL) and Tunable Diode Laser Absorption Spectroscopy (TDLAS) have also been used in monitoring trace gases (water vapour) (Sigrist, 1994). Another system called the Quantum Cascade Laser Open-Path System (QCLOPS) version 2 sensor has been set-up and used to measure the presence of water vapour. Since its first experimental demonstration by Faist et al. (1994), there has been a growing interest in Quantum Cascade (QC) laser-based sensors. In the preceding paragraphs, the conventional and optical methods that can be used to measure water vapour in the troposphere are discussed.

Hygrometers are instruments used to measure the relative humidity of water vapour. Relative humidity, as expressed as a percentage, is the amount of moisture content (water vapour) in air relative to the amount it can hold at a given temperature. The warmer the air is the more moisture it can hold. The hygrometer is composed of two metal plates with a non polymer film between them. The film collects moisture from the air and the moisture causes minute changes in the voltage between the two plates. The changes in the voltages are converted into digital readings which indicate the amount of moisture in the air.

Differential Optical Absorption Spectroscopy (DOAS) is one of the optical techniques used to determine the concentrations of trace gases in the troposphere. The key components of the DOAS system are the light sources which could be thermal light sources such as an incandescent lamps or arc lamp, lasers and natural sources of light such as the sun, moon or the starlight, a reflector to return the light source, a telescope, a spectrometer and a detector.

The light source after passing through several distances in an open atmosphere is collected by a telescope and dispersed by a spectrometer grating. The spectrum projected into the focal plane of the spectrometer is then recorded by a mechanical scanning device in combination with the detector. The recorded spectrum is digitized and transferred to a computer, which analyses the spectral features due to trace gas absorptions along the light path and the concentrations are calculated accordingly.

Differential Absorption Light detection and ranging (DIAL), an optical technique is used to determine the vertical profiles of water vapour, clouds and aerosols by comparing the absorption and scattering of the different laser pulses on these atmospheric species. This technique can be applied in various optical windows such as the Ultraviolet, Visible orthe Infrared regions. Various measurements have been done using various spectroscopic sources. Measurement of water vapour had been made using a temperature-tuned ruby laser operating from 693.7 to 694.5 nm (Zuev et al., 1983). Zuev et al did water vapour measurements up to an open-path length of 10 km. Other measurements of water vapour absorption line at 694.38 nm have been conducted using a ruby laser transmitted to a hard target (Schotland, 1975).

CO_2 lasers was also introduced as a light source in the DIAL technique to measure water vapour with direct detection receiver systems (Murray et al., 1976; Murray, 1978; Rothe, 1980; Baker, 1983). This laser is discretely tunable in the 9.2 to 10.7 µm spectral region due to the overlaps with a number of vibrational and rotational water vapour lines of differing line strengths. Nd: YAG-pumped dye laser has also been used (Cahen et al., 1982; Browell, 1983) to measure water vapour. The dye laser have the advantage of being

4

continuously tuned in the 720 to 730 nm spectral region where water vapour has a number of lines with appropriate line strengths for tropospheric water vapour measurements. Raman lidar can also be used to measure water vapour in the troposphere. This technique takes the advantage of the inverse fourth power of wavelength dependence on Raman scattering cross section. The first Raman lidar measurements of water vapour used the second harmonic of a ruby laser (Melfi et. al., 1969; Cooney, 1970; Cooney, 1971; Pourny et. al., 1980). The advantages of the Raman scattering approach are that the laser source does not have to be tuned to the water vapour absorption line and does not require a very narrow linewidth. This is because the Stokes Raman scattering is temperature independent for tropospheric water vapour. The disadvantage is that the signals are weak. The laser sources used in the DIAL system will be enumerated in chapter two.

Absorption spectroscopy where diode lasers are used in the measurement is called Tunable diode laser absorption spectroscopy (TDLAS). This technique offers high sensitivities for many molecules, high molecular selectivity and a faster response time. The principle of TDLAS is that: a beam of light is transmitted through a target gas in an open-path. One of the absorption lines of water vapour is targeted and the concentrations of water vapour found. In all these optical methods, the concentrations of water vapour are found using the Beer-Lambert equations.

Due to the high cost in building such optical system in measuring the concentrations of trace gases (water vapour) in the troposphere, there is the need to get a sensor that could be used to measure so many gases at the same time. A sensor capable of measuring so many gases at the same time is the

5

Quantum Cascade Laser Open-Path System (QCLOPS) version 2 sensor.This uses a thermoelectrically cooled Quantum Cascade (QC) laser as the spectroscopic source and can have a tunability of up to 50 cm^{-1}or even more (Michel et al., 2010; Holthoff et. al., 2010).

Quantum Cascade (QC) lasers are versatile mid-IR light sources with applications in environment, urban and rural trace gas monitoring. The mid-IR wavelength range of 3-20 µm is a very important region in terms of gas sensing since several molecules such as ammonia (NH_3), ozone (O_3), carbon dioxide (CO_2), water vapour (H_2O) and many molecules have absorption in the mid-IR wavelength range. The mid-infrared region is an important choice for trace gas detection because strong and unique spectroscopic "fingerprints" of most atmospheric trace gases are found.

Moreover, all organic and many inorganic compounds exhibit strong absorption in the spectral region due to their vibrational resonances. These lasers have become a central component in the development of mid-infrared sensing applications due to its high performance.

The QCLOPS version 2 sensor is a mid-infrared laser absorption spectroscopy that uses a thermoelectrically cooled, pulsed Daylight Solutions Inc. QC laser that has a broad tunability from 1020 to 1070 cm^{-1}. The version 2 sensor functions with the same basic principle of absorption spectroscopy where a beam of radiation upon transmission through an open-path medium interacts with medium molecules (can be trace gases (water vapour) or other compounds). Part of the radiation energy is absorbed by the molecules and the remaining part is received by a detector. The main advantages of the QC laser that distinguishes it from the traditional semiconductor laser is its tunability,

higher optical power and the ability to produce light in the terahertz portion of the electromagnetic spectrum. Recently, a number of important trace gases have been measured with QC laser-based sensors (Jimenez et. al., 2004; Taslakov et. al., 2006; Kosterev et. al., 2002; Webster et al., 2001).

Scope of Work

The scope of this work covers the set-up and testing of a Quantum Cascade Laser Open-Path System (QCLOPS) version 2 sensor and a commercial humidity (Campbell CR800) sensor in measuring water vapour concentrations in the troposphere.

Preliminary investigations on gases emitted from the burning of ten different wood species have been studied and the chemical compounds present have been presented in this thesis.

Direct absorption method using the QC laser (Uber Tuner) and Fourier Transform Infrared (FT-IR) spectrometer were used to obtain the infrared spectra of two target gases, 2-Methylphenol and Benzyl alcohol, in the laboratory.

Thesis Arrangements

This thesis is organised as follows: Following introduction in Chapter one, Chapter two gives an overview of semiconductor laser theory and infrared spectroscopy. Chapter three gives a description of the use of Quantum Cascade Laser Open-Path System (QCLOPS) version 2 sensor (second generation sensor) to measure water vapour in the lower atmosphere. It further outlines how selected wood species from Elmina fishing smoking community

were tested for their smoke constituents by Microlab Laboratory in the U.S.A. The chapter is concluded with measuring Benzyl alcohol and 2-Methylphenol with FT-IR spectrometer and a direct absorption method in the laboratory. Chapter four outlines the measurements and results on the version 2 sensor and the commercial humidity sensor. It also reveals the results from the different wood samples received from Microlab Laboratory and final section reports and discusses results obtained from the direct absorption of Benzyl alcohol and 2-Methylphenol. Chapter five gives a summary of the information obtained from the various experiments conducted. Conclusions are drawn and recommendations made for further work are also presented.

CHAPTER TWO

LITERATURE REVIEW

Basic Concepts of laser theory

Lasers are devices that generate coherent light sources by the stimulated emission of radiation (photons) hence the acronym Light Amplification by Stimulated Emission of Radiation. It is this process of amplifying stimulated emission that makes laser light special. A laser consists of the following components as seen in figure 1: (i) a laser medium (i.e. gain medium) which could be a collection of atoms, molecules, ions or in some instances a collection of semiconducting crystals; (ii) a pumping process to excite these atoms (molecules etc) into a higher energy level and (iii) a suitable optical feedback element that allows the beam of radiation to either pass once through the laser medium (as in a laser amplifier) or bounce back and forth repeatedly through the laser medium (as in a laser resonator) .
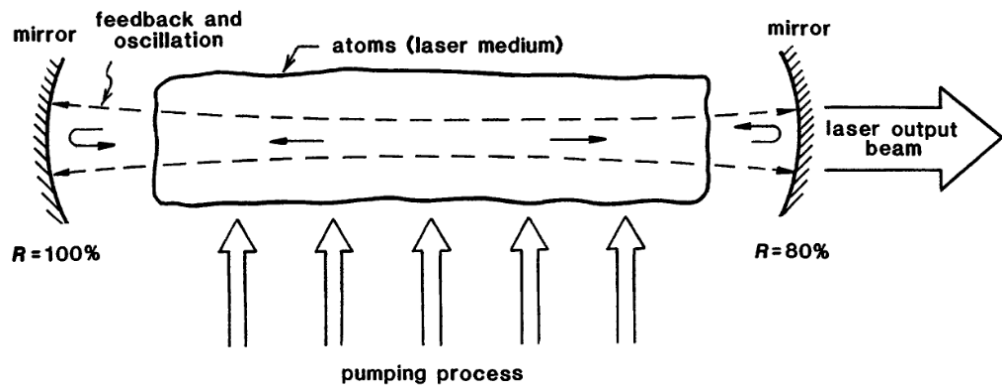
Figure 1: Elements of a typical laser resonator (Siegman, 1986)

9

In general, the gain medium is composed of energy levels where electronic, atomic or molecular transitions result in the emission or absorption of photons. The emission process can be stimulated by radiation, or can spontaneously occur, from the excited state(s) to the lower state(s) and vice versa while the absorption process can only be stimulated from the lower state(s) to the excited state(s) as shown in Figure 2. In interband transitions, the excited states are the conduction band and the lower states are in the valence band while in intersubband transitions the excited and lower states are in the same band (conduction or valence).

In stimulated emission, the generated photons are coherent (i.e. they possess the same frequency, polarization, phase and direction) with the photons in the stimulating radiation. So, an additional photon along with the incident photon is generated. When enough electrons are stimulated, the radiation undergoes amplification. Spontaneous emission on the other hand generates incoherent photons of random phase, polarization, and direction so that the emitted photon does not necessarily add to the radiation. Spontaneous emission occurs because excited energy states are unstable so electrons in the excited states decay to the lower states after a certain period called the lifetime (or recombination time for interband transitions). For emission to be possible, electrons has to be constantly forced or energized through pumping schemes such as optical pumping (i.e .by the continuous wave (cw) or pulsed light emitted by a powerful lamp or a laser beam) and electrical pumping (i.e. by a cw, radio-frequency, or pulsed current flowing in a conductive medium, such as an ionized gas or a semiconductor).
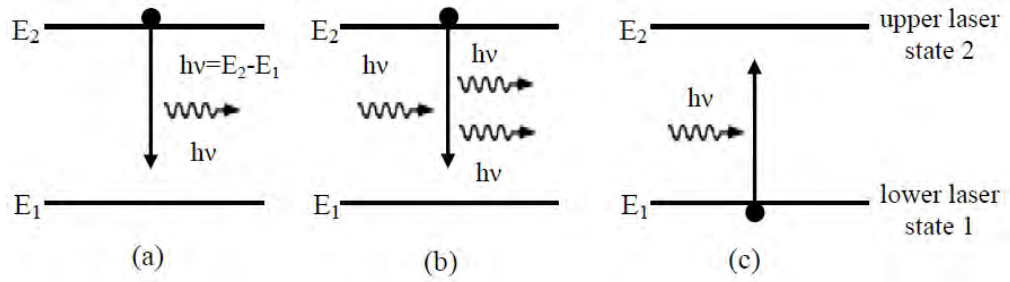
Figure 2: Schematic illustration of the three processes (a) spontaneous emission, (b) stimulated emission (c) absorption (Svelto, 1998)

In optical pumping, an energy state other than the lower state is typically used as the pump reservoir to help increase the efficiency of the pumping scheme for lasing. Light of a particular wavelength matching the separation between the pumping state and the upper state is incident on the gain medium; the electrons absorb the photons and make the transition to the upper state as shown in Figure 3.
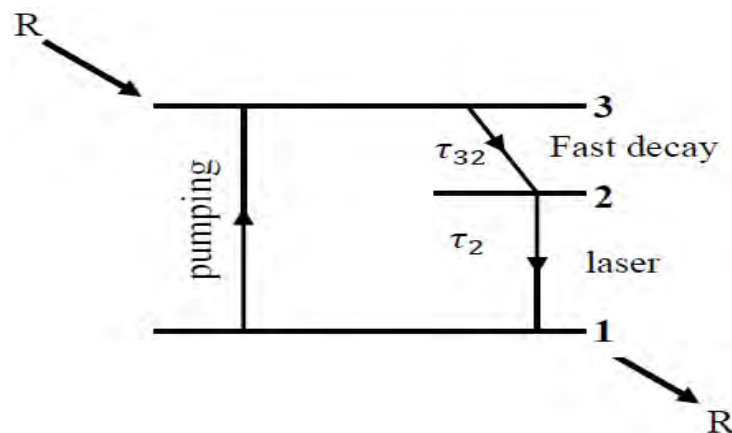
Figure 3: Principle of three-level laser

In order for the excited carriers to undergo stimulated emission, photons matching the energy separation of the laser states must somehow be present in the system. Typically, a laser relies on the spontaneous decay of a few of the excited electrons to emit photons with the desired properties. These emitted photons can then initiate the stimulation process in the medium. But once the stimulation process begins, spontaneous emission becomes an undesirable process because some spontaneously emitted photons will not possess the desired properties and thus noise.

Absorption of the emitted photons is always possible from any two states matching the laser transition as long as there are electrons present in the lower of the two states. If the density of electrons in the lower state becomes comparable to or exceeds the density of electrons in the upper state then the net emission of photons will degrade and the net absorption will increase; hence the optical gain will diminish. So, to maintain a net optical gain the density of electrons in the upper state must always exceed the density in the lower state and this is referred to as population inversion. Population inversion is generally achieved by efficient pumping and slow depopulation of the lower laser state.

The gain medium of the laser is placed in an optical cavity where the laser light bounces back and forth between the mirrors of the cavity thereby enhancing the amplification process through the feedback mechanism. The backward and forward travelling waves of the laser light undergo interference thereby generating standing waves in the cavity. If the interference is destructive the waves cancel each other; hence constructive interference is required for the laser light to be sustained in the cavity. The condition for

constructive interference in the cavity is known as the phase condition and requires the roundtrip phase be an integer multiple of 2π (Verdeyen, 1995; Yariv&Yeh, 2007; Hecht, 1998). With an effective feedback mechanism the amplification process will eventually reach a point where the optical gain equal the losses in the system and this is known as the amplitude (or gain) condition. The phase and gain conditions combine into the oscillation for the laser action given by (Bahaa&Malvin, 1991; Yariv&Yeh, 2007).

$$\underbrace{e^{-i2qL_{cav}}}_{\substack{\text{Phase} \\ \text{condition}}} \underbrace{r_1 r_2 e^{(\gamma - \alpha_{int})L_{cav}}}_{\substack{\text{Gain} \\ \text{condition}}} = 1 \tag{1}$$

where q is the wavevector of the photon (i.e. $q = \frac{2\pi}{\lambda}$), r_1 and r_2 are the amplitude reflection coefficients of the facets, γ is the optical gain coefficient, L_{cav} is the length of the laser cavity, and α_{int} is the internal loss of the laser system. The gain coefficient describes the change in the intensity of the light as it passes through the medium.

i.e

$$\frac{dI}{dz} = \gamma I \tag{2}$$

$$I = I_{(x=0)} e^{\gamma z}$$

From Equation 2, the intensity increases as the light passes through the active medium when the optical gain coefficient is positive. The phase condition, on the other hand, determines the frequency of the photons that the cavity can sustain as given by

$$e^{-i2qL_{cav}} = e^{-im2\pi}, \quad m = 0 \pm 1, \pm 2, \pm 3 \tag{3}$$

$$k = \frac{2\pi n_{eff} \nu}{c} = \frac{m\pi}{L_{cav}}$$

$$\nu = m \frac{c}{2 n_{eff} L_{cav}}$$

where ν is the frequency of allowed photons along the laser cavity (i.e. the longitudinal modes), m is an integer called the mode number, and n_{eff} is the group index of refraction of the modes in the cavity. According to equation 4, multiple modes with mode number m can be sustained in the cavity. The spacing between modes, called the free spectral range is given by

$$\Delta \nu = \frac{c}{2 n_{eff} L_{cav}} \qquad (4)$$

Diode Lasers

Convectional semiconductor lasers, such as, vertical cavity surface emitting laser (VCSELS) and in-plane diode lasers are dependent on the material band gap for their emission wavelength and this is due to the recombination of the electron of the valence band and the hole of the conduction band based on the interband transitions. Figure 4 gives an illustration of the optical transitions in a convectional semiconductor laser. The semiconductor laser consists of a compound of semiconductor, gallium arsenide. This material comes in the form of ingots that are further processed into substrates to which layers of other materials are added. Other materials that can be used to make this type of laser include certain metals (zinc, gold and copper) as additives (dopants) or electrodes and silicon dioxide as an insulator.

A typical semiconductor today consists of a double heterostructure. This consists of several layers of materials that have different functions. The active or light amplification layer is sandwiched between two cladding layers. These cladding layers provide injection of electrons into the active layer.
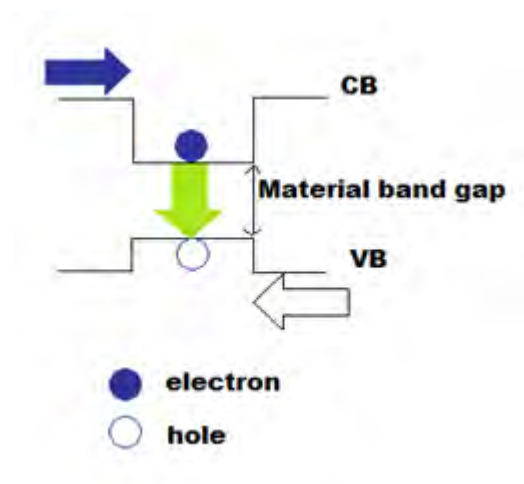
Figure 4: Schematic diagram of the optical transition in a conventional semiconductor

Since the active layer has a refractive index lower than that of the cladding layer, light is confined in the active region.

The performance of a diode laser can be improved by changing the junction design so that diffraction loss in the optical cavity is reduced. This is made possible by modifying the laser and the width of the junction. The index of refraction of the material depends upon the type and quantity of impurity. For example if part of the gallium in the positively charged layer is replaced by aluminium, the index of refraction is reduced and the laser light is better confined to the optical cavity.

The width of the junction can also affect its performance. A narrow dimension confines the current to a single line along the length of the laser, increasing the current density.

Table 1 shows some of the semiconductor lasers and their wavelengths.

Table 1. Diode laser materials and their wavelengths (Hecht, 2008)

Material	Wavelength Range (µm)
AlGaN	0.350- 0.400
GaInN	0.375- 0.440
ZnSSe	0.447-0.480
ZnCdSe	0.490-0.525
AlGaInP/GaAs	0.620-0.680
$Ga_{0.5}In_{0.5}P$/GaAs	0.670-0.680
GaAlAs/GaAs	0.750-0.900
GaAs/GaAs	0.904- 0.900
InGaAs/GaAs	0.915-1.050
InGaAsP/InP	1.100-1.650
InGaAsSb	2.000 -5.000
PbCdS	2.700 -4.200
PbSSe	4.200 - 8.000
PbSnTe	6.500 -30.00
PbSnSe	8.000-30.00

Most of these diode lasers are operated at room temperature with the exception of the infrared diode lasers with wavelength from 2.7-30.0μm, which require some form of cooling in their operations. This is due to their high heat generation, which reduces their efficiency. Diode lasers are good for spectroscopic work due to the following benefits that include high spectral purity, high wavelength stability, high output power, high reliability, and low price.

Neodymium Yttrium Aluminium Garnet, Nd: YAG Laser

The neodymium yttrium aluminium garnet, Nd: YAG laser is a solid state laser using Nd^{3+} ions in a crystalline matrix. The understanding of aNd: YAG laser is best understood using a four-level laser system as described infigure 5.
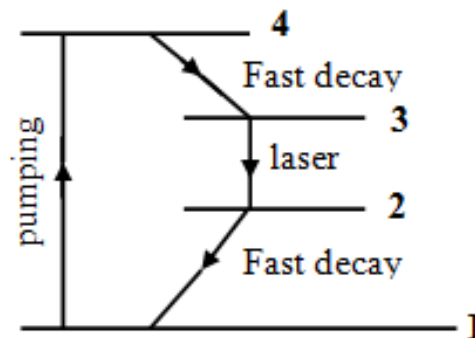
Figure 5: Principle of four-level laser

In a four-level laser, atoms from the ground state energy level 1 are raised to the excited state energy level 4 with the help of optical pumping. From the excited state energy level 4, the atoms nonradiative decays rapidly from energy levels 4 to 3 by spontaneous emission. The transition rate of the

atoms from 4 to 3 is faster as compared with the transition rate of the atoms from 3 to 2. This is due to the fact that the excited state energy level 4 has a shorter lifetime of the order of 10^{-8} seconds (Svelto, 1998). Energy level 3 is a metastable state. Thus the number of atoms in energy level 3 exceeds the number of atoms in level 2. Population inversion is achieved between levels 3 and 2. Laser action takes place between energy levels 3 and 2 by stimulated emission. The atoms from energy level 2 get de-exited to energy level 1. The atoms from energy level 1 are again optically pumped to the energy level 4 and the process continues again.

With the Nd: YAG laser, the lasing medium is a colourless, isotropic crystal of $Y_2Al_5O_{12}$ (Yttrium-Aluminium Garnet-YAG). About 1 % of the Yttrium is replaced by Neodymium. The energy levels of the Nd^{3+} ions are responsible for the fluorescent property that is the active properties in the amplification process.

Population inversion results from the shinning of light onto the crystal. If the light is intense enough, atoms within the crystal absorbs the light transition from the ground state into the absorption bands (excited state). This is done using a flash lamp-often a quartz tube filled with a noble gas through which high energy is stored in a capacitor is discharged emitting in the blue and ultraviolet.

Dye Lasers

Dye lasers are lasers that use an organic dye as the lasing medium, usually a liquid solution (methanol or ethanol). The dyes used in these lasers contain large organic molecules that fluoresce when exposed to the

appropriate frequency of light. The incoming light excites the dye molecules, which emit stimulated emission as long as the molecules remain in their initially-formed singlet state. In this situation, the molecules emit light via fluorescence, and the dye is quite clear to the lasing wavelength. Within a microsecond or less, the molecules change to their triplet state. In the triplet state, light is emitted via phosphorescence and the molecules begin to absorb the lasing wavelength, making dye opaque. Liquid dyes have extremely high lasing threshold.

Since organic dyes tend to degrade under the influence of light, the dye solution is circulated from a large reservoir (Schafer &Drexhage, 1977). The dye solution could be also flow through a cuvette that is a glass container. These advantages come at the cost of a more complicated alignment.

Liquid dyes have very high laser medium. The beam only needs to make a few passes through the liquid for high gains in power and hence the high transmittance of the output coupler. This high gain nature leads to very high losses, as any reflections generated by the dye cell walls will dramatically reduce the amount of energy available to the beam. Therefore pumping cavities are coated, anodized or made of materials that can absorb the lasing wavelength while effectively reflecting the pumping energy (Svelto, 1998).

Ruby Lasers

Ruby is an aluminium oxide crystal in which some aluminium atoms have been replaced with chromium atoms. Chromium gives ruby its characteristic red colour and is responsible for the lasing behaviour of the

crystal. Chromium atoms absorb green and blue light and reflect only red light.

For a ruby laser, a crystal of ruby is formed into a cylinder. A fully reflecting mirror is placed at one end and a partially reflecting mirror on the other. A high intensity lamp is spiraled around the ruby cylinder to provide a flash of white light that triggers the laser action. The blue and green wavelengths in the flash excite electrons in the chromium atoms into a higher energy level. Upon returning to their normal state, the electrons emit the characteristic ruby-red light.

The mirrors reflect some of this light back and forth into the ruby crystal, stimulating other excited chromium atoms to produce more red light, until the light pulse builds up to a high power and drains the energy stored in the crystal. The optically pumped solid-state laser uses Sapphire as the host lattice and chromium as the active ions.

Titanium-Sapphire Lasers

Titanium-Sapphire lasers are tunable lasers which emit red and the near-infrared light. These lasers are used in scientific research because of their tunability and the ability to generate ultrashort pulses. Titanium-Sapphire refers to the lasing medium where the crystal of Sapphire (Al_2O_3) is doped with Titanium ions. It is usually pumped with another laser with a wavelength of 514 to 532 nm, for argon lasers are used. This laser operate most efficiently at wavelength near 800 nm.

One disadvantage of these laser sourcesare that it does not have broad tunability thereby allowing multiple gas specie to be detected. One laser that

has the ability to tune over wide range of wavelength is the Quantum Cascade (QC) laser.

Quantum Cascade (QC) Lasers-General Overview

Quantum Cascade (QC) lasers are unipolar semiconductor injection lasers with the emission wavelengths in the mid-infrared and far-infrared based on intersubband electron transitions in a multiple quantum well heterostructure. In a unipolar QC laser, once an electron undergoes an intersubband transition and a photon is emitted, the electron moves into the next period of the structure where another photon is emitted. The phenomenon of a single electron causing emission of multiple photons as it moves through the QC laser structure gives rise to the name ''Quantum Cascade'', as seen in Figure 6.

The concept of QC lasers was first proposed by Kazirinov&Suris (1971) in a seminal paper where light was amplified by ''photon-assisted'' tunnelling in quantum well (QW) superlattice was described. Several advances in high quality heterostructure growth and band structure engineering led to the first demonstration of the QC lasers at $\lambda \approx 4.3$ µm by J. Faist et al. (1994) at Bell Labs using $In_{0.47}Ga_{0.47}As/In_{0.52}Al_{0.48}As$ alloy lattice matched on an InP substrate (Faist et. al., 1997). Since then, significant improvement has been achieved for QC lasers regarding to their performance and functionality. The timeline of major achievements in the development of the QC lasers, includes distributed feedback (DFB) QC lasers (Faist et al., 1997), ''bow-tie'' QC lasers (Gmachl et. al., 1998), broadband QC lasers (Gmachl et. al., 2002), terahertz QC lasers (Kohler et. al., 2002; Williams et. al., 2003), nonlinear QC

lasers (Owschimikow et. al., 2003; Gmachl et. al., 2003), high power room-temperature continuous-wave (CW) QC lasers (Beck et. al., 2002; Yu et. el., 2003), QC lasers grown by metal organic chemical vapor deposition (MOCVD) (Roberts et. al., 2003), QC lasers based on GaAs/AlGaAs material system (Sirtori et. al., 1998), and very recently InAs/AlSb-based QC lasers for shorter wavelength generation (Devenson et. al., 2007), among others.
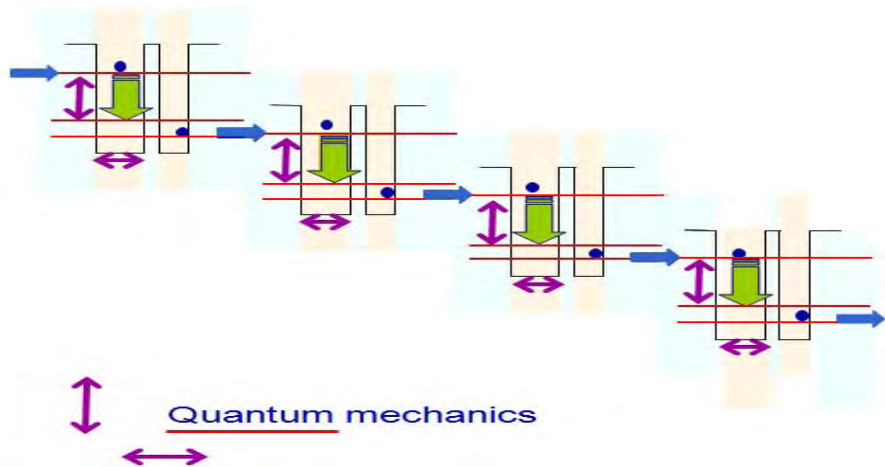
Figure 6: ''Quantum Cascade'' Schematic diagram showing electron flow through the quantum wells to emit several photons on the way

Design and Principles of Quantum Cascade (QC) Lasers

Quantum cascade lasers are based on hundreds of engineered semiconductor layers. Typically, two semiconductor materials with band-gaps and sufficient offset between them (Figure 7) are used to create a system of quantum wells and barriers. The potential corresponding to this complex system can be solved using theSchrödinger's time-independentequation:
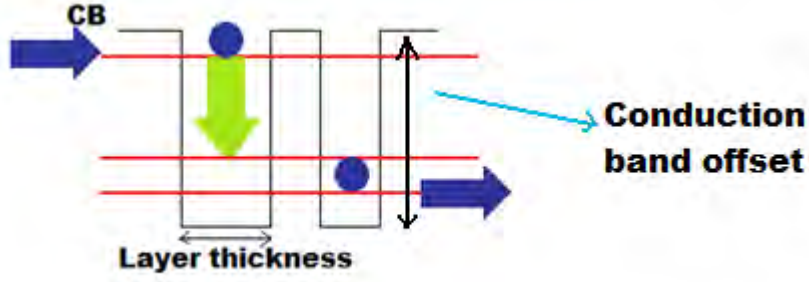
Figure 7: Schematic diagram of a coupled QW with conduction band offset defined by the black arrow and the blue arrow shows the electron travel path in the quantum wells where the optical transition takes place

$$\left(-\frac{\hbar^2}{2m^*}\nabla^2 + V\right)\psi = E\psi \qquad (5)$$

where, $\hbar$ is the planks constant, m^* is the effective mass of the electron, and V is the potential function of the semiconductor layers under an electric field. The eigenvalues of equation 5 give the energy levels, E_i, and the eigenvectors give the wavefunctions, ψ_i.

The wavefunctions can be used to show the probability, P_x of an electron located between positions x_1 and x_2.

$$P_x = \int_{x1}^{x2}\psi^*_i\psi_i dx \qquad (6)$$

Where ψ_i^* is the complex conjugate of ψ_i. When $\psi_i^*\psi_i$ is plotted, regions with a larger ''area under the curve'' correspond to regions where electrons are more likely to be found. When designed properly, the energy levels and wavefunctions of a QC structure create two distinct regions: (1) the active region and (2) the injector region. The active region generates photons by

achieving a population inversion between the upper laser level and the lower level by pumping into the upper level and rapidly extracting electrons from the lower level. The primary function of the injector region is to move electrons from the lower laser level of one active region to the upper laser level of the next down-stream active region. Essentially, the goal of the injector is to efficiently recycle ''used'' electrons so they can undergo additional optical transitions.

Figure 8 shows a typical energy of two stages of QC laser structure. The conduction band edge is given by the solid black lines. The tilt in the conduction band is due to an electric field that is applied over the laser; in this example, we assume that the electric field is homogeneous. The electrons enter the structure from the left, cascade through the injector energy levels, make optical transitions (marked by vertical arrows), and exit out to the right. After the design process, the QC band structures are grown by molecular beam epitaxy (MBE) or by metal organic chemical vapour deposition (MOCVD). The latter method is used mostly in industry because of the higher growth rates and the near-ambient pressure growth conditions. The QC wafer is processed into a laser ridges and for devices requiring improved heat extraction (i.e devices at room temperature in continuous wave mode), a thicklayer of gold (~ 5µm) is electroplated on the top of the laser ridge (Yu et. al., 2003; Liu et. al., 2006). For improved heat extraction from the device, buried heterostructure (BH) devices can be processed using additional growth step beyond the initial QC fabrication. The devices are then mounted to a heat sink. For applications where thermal effects are not an issue, the devices can be mounted epitaxial sit up. However, applications requiring superior heat

extraction benefit significantly by moving the epitaxial side in contact with the heat sink.
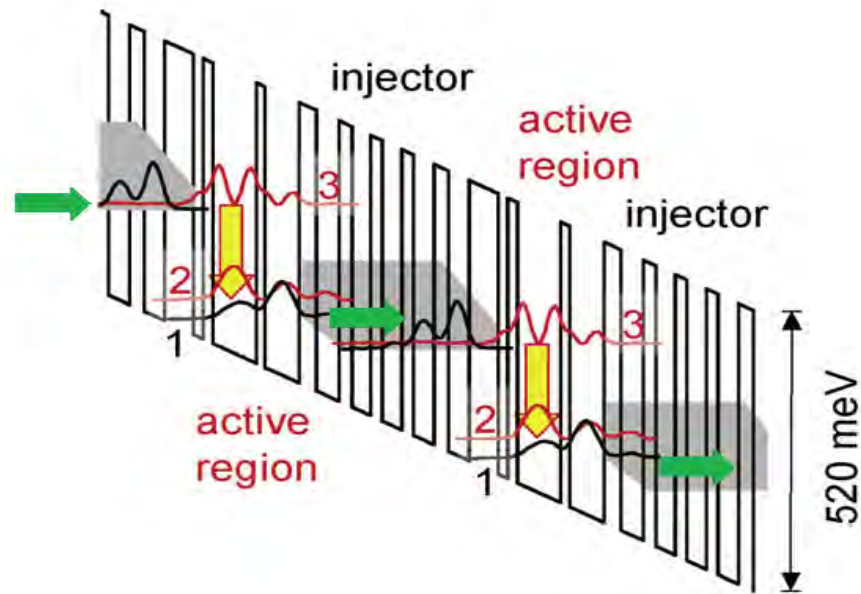
Figure 8: Energy diagram for a typical QC laser. The yellow vertical arrows indicate the optical transitions, the injector regions are shaded in gray and the red and black horizontal arrows cascading through the medium (Curl et. al., 2010)

Spectroscopy

Spectroscopy is the study of the interaction between matter and radiated energy. The study of spectroscopy originated from the dispersion of visible light according to its wavelengths by a prism. Later, this concept was broadened to comprise any interaction with radiative energy.

The electromagnetic spectrum is a seemingly diverse collection of radiant energy, from the cosmic rays to X-rays to visible light to microwaves, each of which is considered as a wave or particle travelling at the speed of

light. These waves differ from each other as illustrated in figure 9. Spectroscopy can be performed in any particular region of the electromagnetic spectrum. Spectroscopy in the X-ray, ultraviolet and visible, infrared, microwave and radiofrequency are respectively called X-ray spectroscopy, UV-Visible spectroscopy, Infrared spectroscopy, Microwave spectroscopy and Radiofrequency spectroscopy.

X-Ray Spectroscopy

X-ray spectroscopy is one of the spectroscopic techniques used in determining the electronic structure of materials by using X-ray excitation. X-rays are produced by the bombardment of a solid by electrons with energy of a few kilo-electron volt (keV) or more. The radiation is made up of a continuous part (Bremsstrahlung) which is generated by a charged electron that undergoes a deceleration and a change in the direction of motion of the atoms and the discrete part (characteristic) of the radiation is the line spectrum that is a characteristic part for a particular material. The result of the bombardment knocks of the inner shell of the atom.

Microwave Spectroscopy

Microwave spectroscopy is the interaction of matter and electromagnetic radiation in the microwave region of the electromagnetic spectrum. The interaction of microwaves with matter can be detected by observing the attenuation or phase shift of a microwave transition. Microwave spectroscopy has been used for the precision determination of spins and moments of nuclei (The free dictionary. n.d.). It has also contributed to the

information of the moment of inertia and the spin-rotation coupling mechanisms (The free dictionary. n.d.).
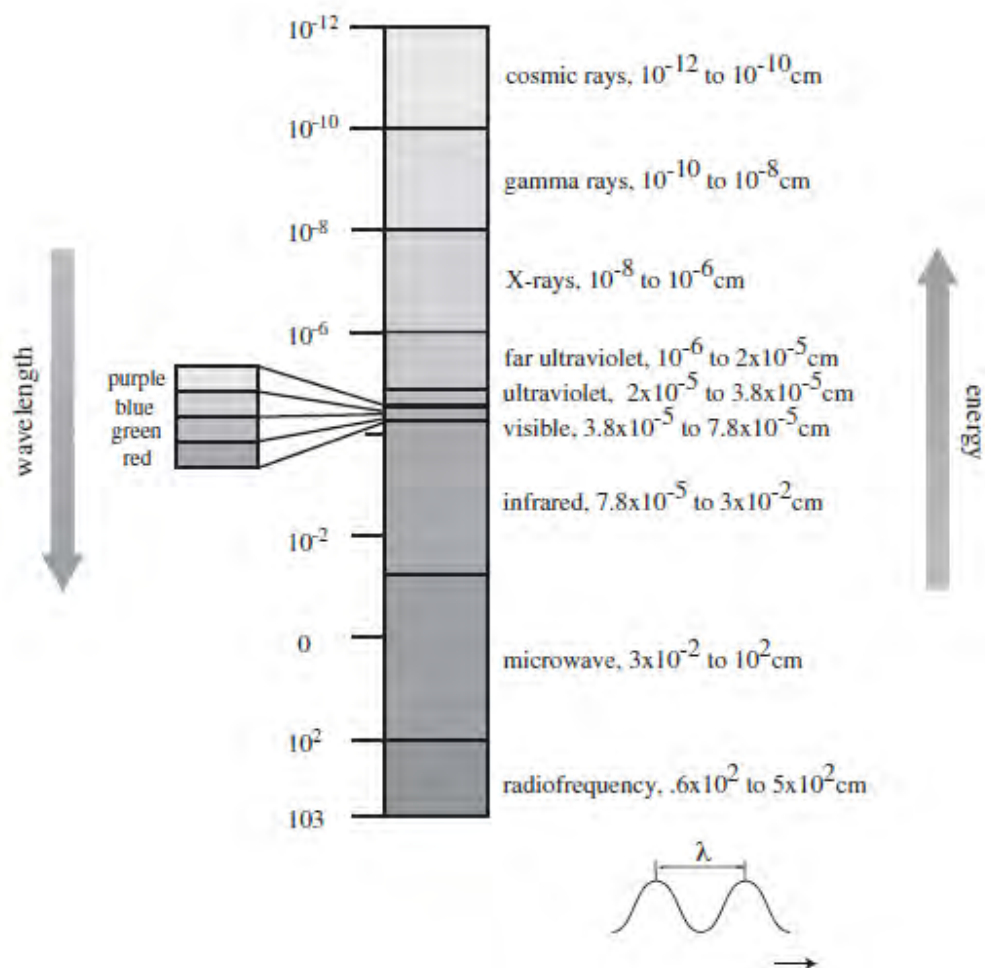
Figure 9: The electromagnetic spectrum

Infrared Spectroscopy (IR)

Infrared (IR) spectroscopy is one of the most versatile and useful techniques used for quantitative and qualitative characterization of many types of materials found in solids, liquids or gaseous state. The IR region is divided into three regions: the near, mid, and far IR (Figure 10). An infrared spectrum is obtained by passing an infrared radiation through a sample and determining

what fraction of the incident radiation is absorbed by a particular energy. This kind of spectroscopy is called absorption spectroscopy. The energy at which the peak in the absorption spectrum appears corresponds to the frequency of vibration of the sample molecule.

	λ, cm	λ, μm	λ, cm^{-1} (wavenumber)	energy (E)
NEAR	7.8x10-5 to 3x10-4 (.000078-.0003)	0.78 to 3	12820 to 4000	10-37 Kcal/mole
MID	3x10-4 to 3x10-3 (.0003-.003)	3 to 30	4000 to 400	1-10 Kcal/mole
FAR	3x10-3 to 3x10-2 (.003-.03)	30-300	400 to 33	0.1-1 Kcal/mole
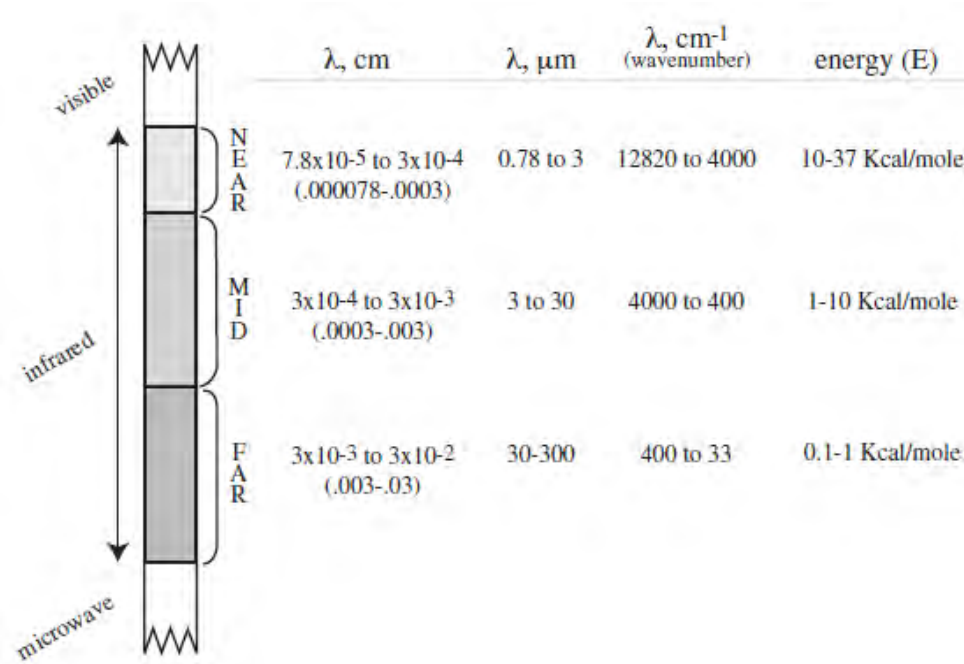
Figure 10: The IR regions of the electromagnetic spectrum

Theory of IR spectroscopy

For any molecule to show infrared absorptions, then the electric dipole moment of the molecule must change during the vibration (Stuart, 2004). The frequencies of these vibrations fall within the IR region of the electromagnetic spectrum from 14000 to 20 cm^{-1}. The most useful range for general problem solving lies between 4000 and 400 cm^{-1}, the mid-IR range. When a sample is irradiated with IR energy, the energy coincides with the vibrational frequencies of the functional groups within the molecule. These vibrations cause a change in the dipole moment of the molecule, giving rise to the

absorption of IR. The absorption of IR of any molecule therefore gives a unique tool for identification of any particular compound whether known or unknown.

Applications of Mid-Infrared Portion of the Spectrum

There are many applications of the mid-IR portion of the electromagnetic spectrum. One application is as a result that most gases of interest, such as Ozone, Ammonia, Carbon monoxide and Carbon sulphide have their absorption fingerprint features in this portion of the spectrum (Filho et. al., 2006; Jimenez et. al., 2003; &Taslakov et. al., 2006). This means that each gas has a unique characteristic wavelength in which they can be tuned to in order to sense them. In addition to trace gas sensing, the mid-IR portion of the spectrum is important because metal detection occurs in this portion of the spectrum (due to the fact that all bodies give off infrared radiation) (Arthur, 2003). Distant space objects also give off light in this portion of the spectrum hence provides an important tool for astronomers.

Direct Absorption Spectroscopy

Direct Absorption Spectroscopy is a technique for absorption based measurements because of its simplicity, accuracy, and ability to make absolute measurements. Direct absorption spectroscopy technique is used for studying the absorption of small molecules at low to moderate pressures. The amount of light that is transmitted through a sample can be measured in a direct absorption method.If the light source is tunable and monochromatic (laser), one can record the absorption spectrum of the sample by recording the

transmitted intensity as a function of frequency. Alternatively, a broad light source can be used when the incident light or the transmitted light is spectrally dispersed (Fourier Transform (FT-IR) Spectroscopy).

A drawback of direct absorption spectroscopy might be its limited sensitivity. A small attenuation of the light intensity has to be measured on top of a large background of the incident light. Additionally, intensity fluctuations of laser can be rather large (up to 50%), thereby obscuring the absorption signal. Although one can correct these pulse-to-pulse fluctuations, significantly better results are obtained when more stable light sources, such as continuous wave (cw) instead of pulsed, are used.

Beer-Lambert law

The Beer-Lambert law is used to relate the amount of light transmitted by a sample to the thickness of the sample. Figure 11 shows a monochromatic light of intensity I_o impinging on a sample of thickness l.The sample can be a solid, liquid or gas. An intensity$I$ is transmitted through the sample. The absorbance is directly proportional to the thickness (pathlength) and concentration of the sample and is given by

$$A = \mu c l \qquad (7)$$

where$A$ is the absorbance of the sample, c the concentration and l the pathlength of the sample. The constant of proportionality μ is referred to as the absorption coefficient and it is the characteristic property of any specie. It depends strongly on the frequency or wavelength of the light source and can be measured in the laboratory.The absorbance is equal to the difference between the logarithms of the intensity of light entering the sample (I_o) and

(13)

the intensity of the light transmitted (I) by the sample. Absorbance is a dimensionless quantity.

$$A = log I_o - log I = \log (I_o/I) \qquad (8)$$
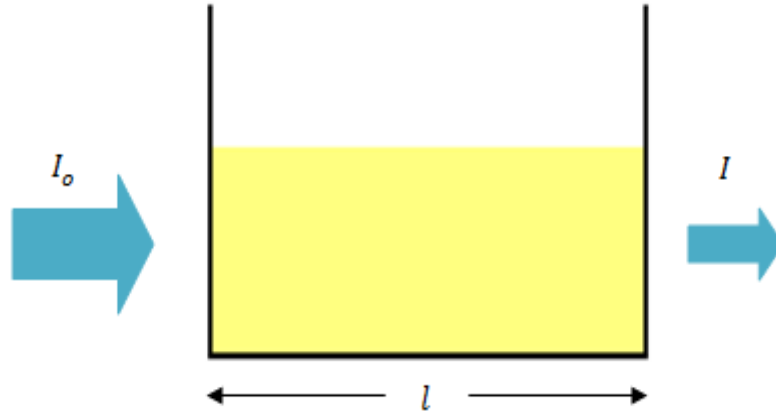
Figure 11: Illustration of the Beer-Lambert law

From Beer-Lambert law it can be seen that an increase in the absorption path length results in a stronger absorption signal. The absorption path length can be increased in a way using a 'multipass'-cell configuration e.g. White cell (White, 1942) or a Herriott cell (Herriott et al., 1964). A 'multipass'-cell consists of two or more highly reflective mirrors between which the light is reflected many times, thereby traversing a different optical path upon each reflection. The sample of interest is placed between the mirrors and absorption path lengths of a few hundred meters can be achieved.

The above equations (equations 7 and 8) work well for solids and liquids but in considering gases certain factors need to be added to the Beer-Lambert in equation 7. The ideal gas law relates to the physical properties of a gas to its concentration. The law states that:

$$PV = nRT \qquad (9)$$

where P is the pressure, V the volume, n the number of moles, R the universal gas constant and T the temperature. From equation (9) the concentration c is given by $c = {}^{n}/_{V}$. With these equations the concentrations of a gas can be written as:

$$A = {}^{Pl\mu}/_{RT} \qquad (10)$$

For gases the absorbance depends also on the pressure and the temperature of the gas.

The Beer-Lambert law however has some limitations. These are due to instrumental or chemical effects.

These limitations include:

- Deviations in absorption coefficients at high concentrations as illustrated in figure 12. This is due to electrostatic interactions between molecules and changes in refractive index.
- Scattering of light due to particulates in the sample.
- Florescence or phosphorescence of the sample
- Stray light.

The effect of these limitations can be minimized by avoiding reflecting surfaces around experimental set-up.
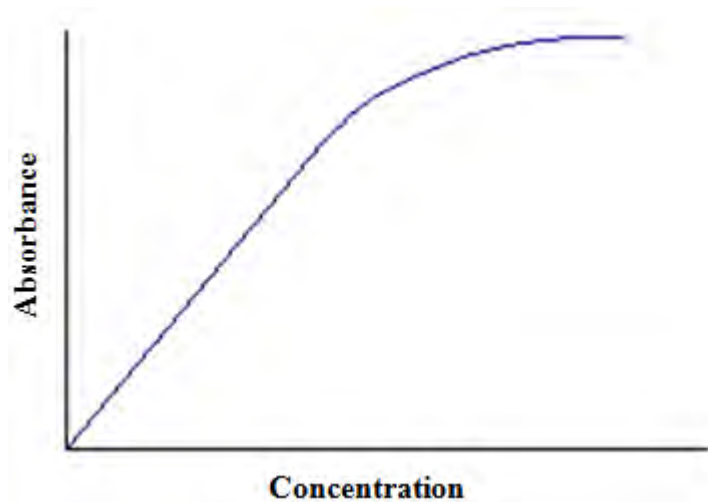
Figure 12: A plot ofabsorbance against concentration

IR absorptions are generally presented as either wavenumbers or wavelength. Wavenumber is defined as the number of waves per unit length. Thus wavelength is directly proportional to the frequency, as well as the energy of IR absorptions. IR absorption information is generally presented in a form of a spectrum with wavelength or wavenumber as the x-axis and absorption intensity or percentage transmittance as the y-axis (Figure 13 and 14).
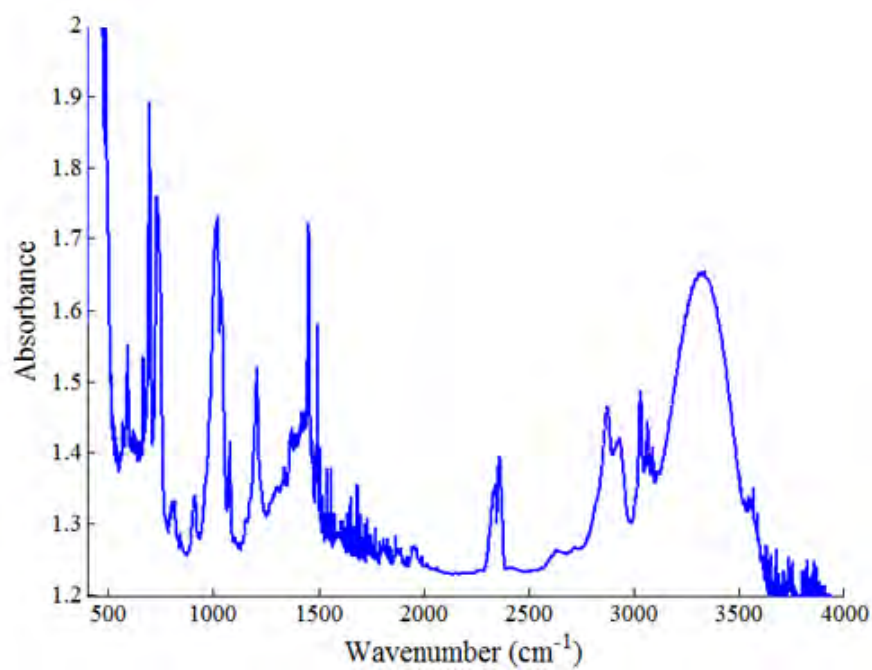
Figure 13: The IR spectrum of Benzyl alcohol plotted as Absorbance against wavenumber
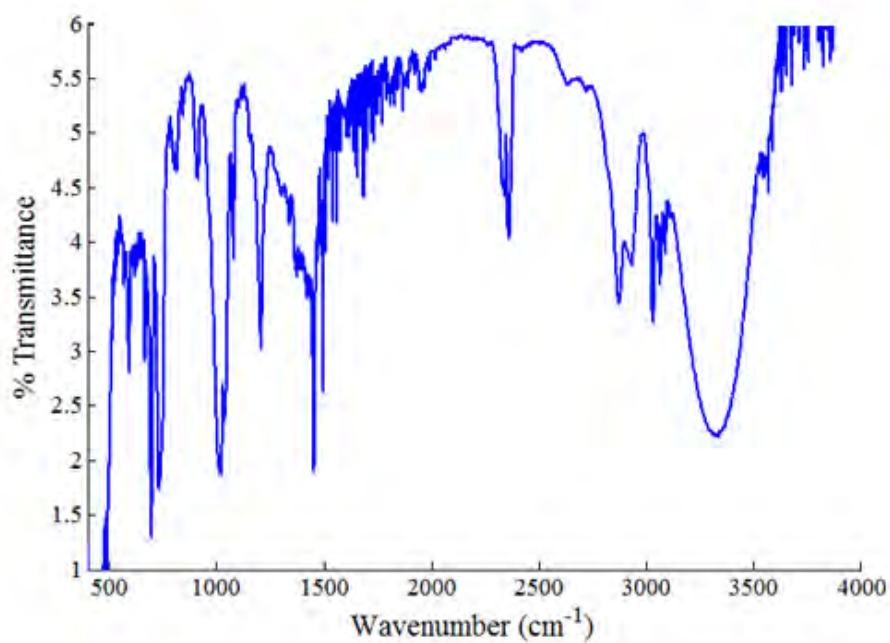
Figure 14: The IR spectrum of Benzyl alcohol plotted as percentage transmittance against wavenumber

CHAPTER THREE

EXPERIMENTAL SET-UP AND PROCEDURES

A detailed description of a Quantum Cascade Laser Open-Path System (QCLOPS) version 2 sensor and its experimental procedures are given in this chapter. The chapter has been arranged in the following order. The first part describes the set-up and use of the QCLOPS version 2 sensor (second generation sensor), a modification of a first design (Michel et al., 2010), to monitor water vapour in the troposphere. The second part outlines wood species sampled from Elmina fishing smoking community, sent to Microlab Laboratory in the U.S.A for chemical test. Lastly, the chapter looks at how gaseous Benzyl alcohol and 2-Methylphenol were measured with a Fourier Transform Infrared (FT-IR) spectrometer and a direct absorption method in the laboratory.

Description of the QCLOPS version 2 sensor

There are several components making up the version 2 sensor. The main components are a Quantum Cascade (QC) laser, beam expander, thermoelectrically cooled (TE) detector, a He-Ne laser, lens, and five types of mirrors. The mirrors comprise of a dichroic mirror, 8   parabolic mirror, elliptical (launch) mirror, plane mirror and a corner cube mirror (retroreflector).Figure 15 shows the schematic diagram of version 2 sensor with ray traced through its components and plate 1 show a picture of the

experimental setup. The version 2 sensor was used for measuring water vapour in the troposphere.
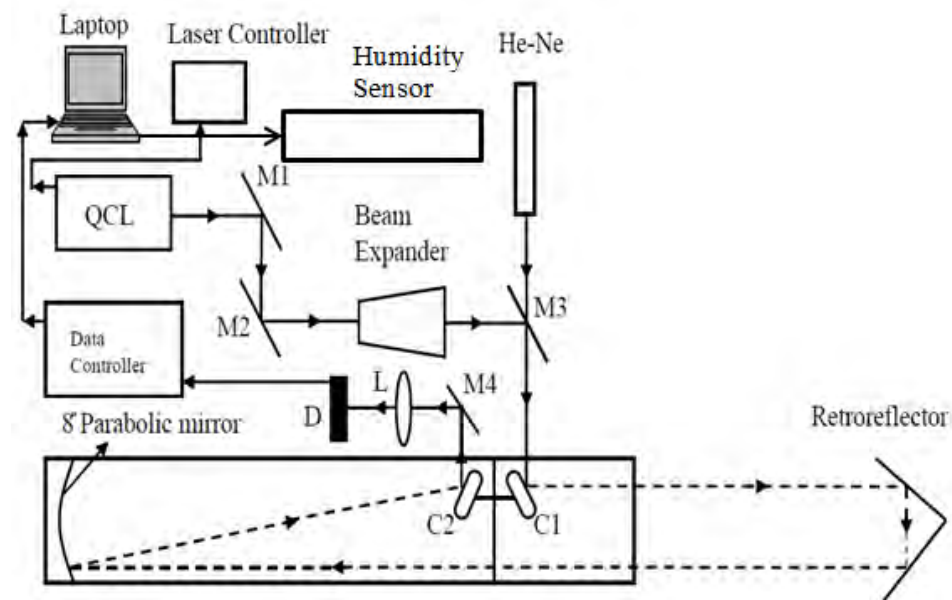
Figure 15: Schematic diagram of QCLOPS version 2 sensor. M1, M2 & M4 – PlaneMirrors, M2 - Dichroic mirror, C1 & C2 - Elliptical mirrors, L - Lens, D - Vigo Detector

The version 2 sensor (plate 1) used a thermoelectrically cooled, pulsed QC laser (Daylight Solution Inc). The QC laser had an average maximum power of 5 mW at 5 % duty cycle. Its wavelength tunability was from 1020 cm^{-1} (9.8 µm) to 1070 cm^{-1}(9.3 µm) with a centre wavelength of 1045 cm^{-1} (9.5 µm). The direct absorption method used in measuring Benzyl alcohol and 2-Methylphenol used a tunable pulsed External Cavity Quantum Cascade Laser (ECqcl^{TM}) (Uber Tuner) with an average maximum power of 400mW at 5 % duty cycle. It had broader wavelength tunabilityfrom 965 cm^{-1}

(10.3 µm) to 1260 cm^{-1} (7.9 µm) with a centre wavelength of 1112.5 cm^{-1} (8.9µm).
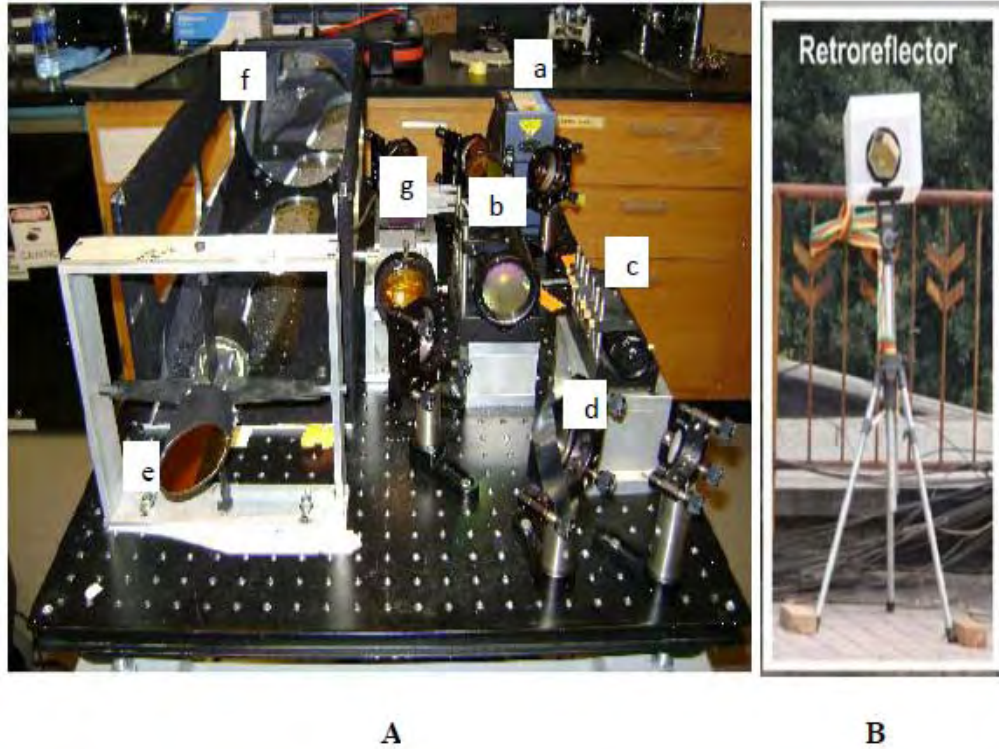
Plate 1: (A) QCLOPS version 2 sensor, a - QC laser, b- Beam expander, c - He-Ne laser, d - Dichroic mirror, e - Elliptical mirror, f - 8 launch mirror, g - Vigo Detector (B) Retroreflector

These QC lasers were designed to be small and compact. They utilized specially designed miniature lenses to optimize system performance and also incorporate thermoelectric cooling (TEC) technology. This controls the temperature of the laser so that no cryogenic cooling is required.

The He-Ne laser (Thorlabs LDM635) was used as an alignment laser in the version 2 sensor. It was a continuous wave laser with 4.5 mW maximum output power. It had a single longitudinal mode (TEM$_{00}$) with a beam divergence of 1.00 mrad. The QC laser was directed to follow the path of the

He-Ne laser's beam since the QC laser was invisible to the eye. The He-Ne laser was made to incident on the Dichroic mirror (M3). The M3 was placed at an angle of 45° to the QC laser beam path as seen in figure 15. The function of this mirror was to reflect certain wavelengths (QC laser) and transmit others (He-Ne laser). The He-Ne upon transmitting through M3 was made to reflect on an elliptical mirror C1, at angle suitable for good reflection from the retroreflector which was placed at a distance from the system. This retroreflector is a set of three gold coated mirrors perpendicularly attached to each other forming the retroreflector or corner-cube. The reflected beam upon entering the version 2 sensor from the retroreflector was made to incident on an 8 parabolic mirror placed adjacent to QC laser (see plate 1).

The 8 parabolic mirror focused the reflected light from the retroreflector unto the second elliptical mirror C2, which then reflected the light unto a plane mirror (M4). The lens (L) then focused the light from M4 unto the thermoelectrically cooled (TE) Vigo detector (VIGO PCI-2TE/VPAC-1000). The Vigo detector had a built in preamplifier (model STCC) designed to obtain high performance. This ensured stability in all conditions and had a high signal to noise ratio. The signal was then communicated to the data controller (PXI-1033) via a laptop computer for data storage and analysis of the signal.

Once a good signal had been achieved with the He-Ne, the computer operated QC laser was switched on and with little optical adjustments from M1 and M2 a good signal is obtained which goes through the beam expander (Special Optics 53-50-10X). The beam expander had transmission greater than 97 % and had adjustable lens spacing with a Zinc Selenide (ZnSe) element

that enables low insertion loss over a spectral range from 9.0 to 10.6 µm. The expanded beam was incident on the dichroic mirror (M3) and reflected to follow the path of the He-Ne. In the version 2 sensor deployment, the retroreflector was place at a distance of 41.5 m away from the system, thus giving a total optical pathlength of 83.0 m.

All data were collected with the help of a National Instruments data controller which included a high speed digitizer (PXI-5105) and a serial controller (PXI-8430) used to control the tuning and to digitize the VIGO detector signal. The data were collected via a LabView 8.5 software (National Instrument). A complete scan of the QC laser with its data collection took approximately 8 minutes. For every tuning of the QC laser, 1000 pulses were sent to the retroreflector and back within a second with the mean and standard deviations recorded.

A Commercial Relative humidity sensor (Campbell CR800) was placed 2.0 m away from the QCLOPS sensor and simultaneously logged. A Nicolet NEXUS 870 FT-IR spectrometer was used to scan the absolute emission wavelengths of the QC laser for calibration of the operational wavelength with respect to the wavelength displayed on the laser controller (Daylight Solutions TLC 1001).

Processing the Wood Species to Sawdust

Ten different wood species were obtained from Elmina fishing smoking community from the period of July to October 2009. These wood species were chosen based on their availability at the time of collection and

the frequency at which they were used by the women (fishmongers') to smoke their fish.

The wood species were Mango (Magiferaindica), Yaya (Amphimapterocarpodes), Konkroma (Morindalucida), Esia (Petersianthusmacrocarpus), Esakokoo (Celtiszenkeri), Dwindwinaba (Leucaniodiscuscupaniodes), Emire (Terminaliaivorensis), Cocoa (Theobromacacoa), Aborday (Azadirachtaindica) and Kroma (Klainedoxagabonensis). These wood species were sent to the forestry commission where they were certified and cut into small logs each weighing about 20.0 g.

The logs were sawed to sawdust constituents and bagged in transparent polystyrene bags (plate 2) which were sent to Microlab Laboratory (an analytical chemistry company) in the U.S.A where chemical test were carried out. Each labelled bag contained both the stem and the bark of the log sample.

Plate 2: Bagged wood samples after sawing to sawdust
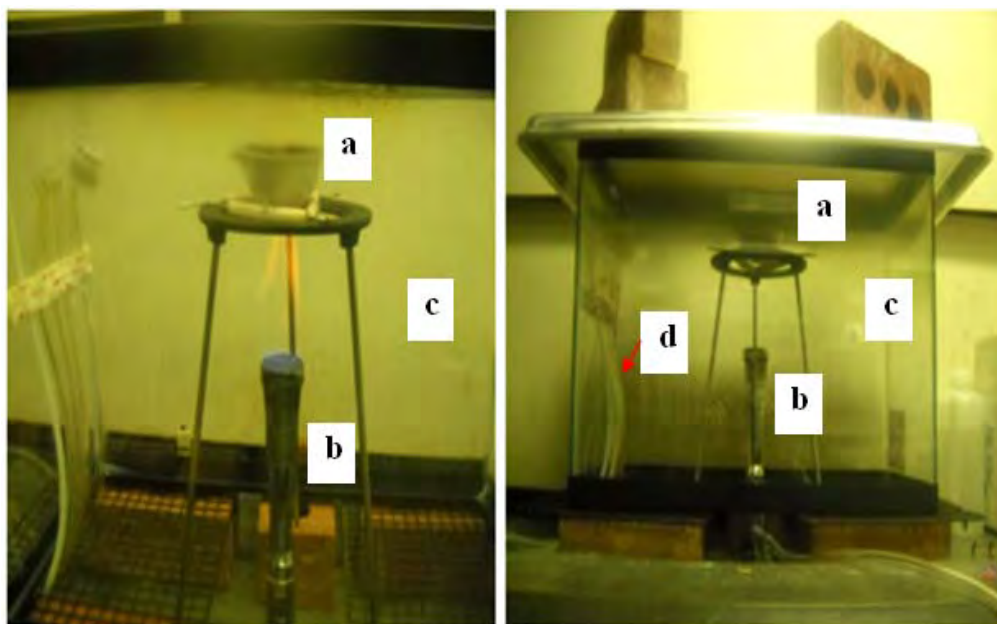
Plate 3: Enclosure used for wood analyses - (a) crucible for holding sawdust during burning (b) bunsen burner (c) aquarium (d) tubes for collecting gases for characterization

Plate 3 shows the enclosure used by Microlab laboratory for the burning and collection of the smoke for the analysed wood samples. The different wood species (sawdust constituents) were simultaneously placed in a crucible. The bunsen burner was placed directly under the crucible and turned on. The sawdust turned into smoke and it was collected via tubes to be analysed.

Fourier Transform Infrared (FT-IR) Spectrometer

The Nicolet NEXUS 870 FT-IR Spectrometer is an instrument used for measuring the infrared spectra of compounds (solids, liquids or gases). The instrument consists of two major components namely the optical system and a computer to operate and visualize the data. The optical system consists of a

He-Ne laser, interferometer, beamsplitter, Infrared (IR) source, detectors and mirrors as shown in figure 16. Figure 17 shows a schematic diagram of the interferometer.
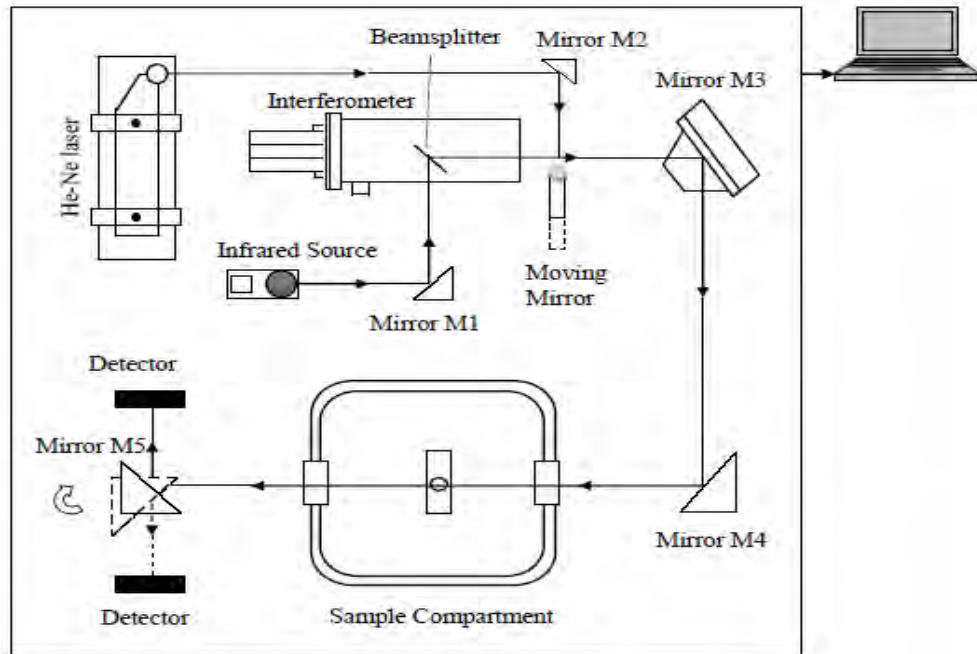
Figure 16: Schematic diagram of FT-IR spectrometer showing ray tracing from the infrared source to the detector
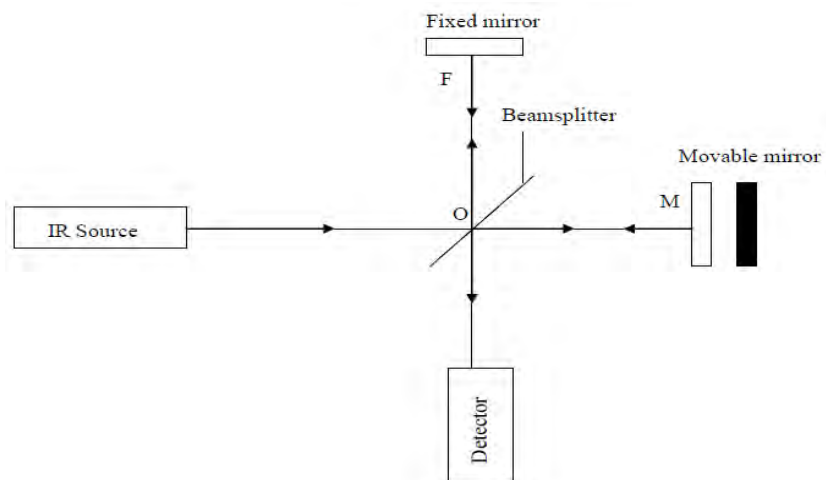
Figure 17: Schematic diagram of Michelson Interferometer

The infrared (IR) source in the FT-IR is made of different materials depending on the wavelength region. FT-IR spectrometers use Globar or Nernst sources for the Mid-IR region. Far-IR and Near-IR regions use a high-pressure mercury lamp and tungsten-halogen lamps respectively. All the surfaces of the mirrors in the interferometer are coated with gold for high reflectivity for the infrared source. Infrared radiation produced by the source is directed onto mirror M1, which reflects the beam into an interferometer. The interferometer consists of two mutually perpendicular plane mirrors, one of which moves along an axis which is perpendicular to its plane (Figure 17). Bisecting the fixed mirror is a laminate material called the beamsplitter which is made of Extended Range Potassium Bromide (XT-KBr) (11,000 to 375 cm^{-1}) which reflects and transmits IR light equally. The collimated beam from the IR source is partially reflected (50 %) to a fixed mirror, F and partially transmitted (50 %) to the movable mirror, M. The two IR beams are then reflected back to the beamsplitter by the mirrors, F and M. The recombination of the two beams at the beamsplitter causes the beam to interfere with each other whether constructively or destructively depending on the wavelength of the IR (frequency in wavenumbers). The infrared beam exits the interferometer and is reflected by two mirrors, M3 and M4 which sends the beam through the sample compartment to the detector. The sample compartment is the arena where samples are placed to determine its IR spectra. There are two types of detectors used namely a room temperature DeuteratedTriglycineSulfate (DTGS) and the liquid nitrogen cooled Mercury-Cadmium-Telluride (MCT). The detector produces an electrical signal in response to the encoded radiation striking it. This measures the total intensity

of infrared radiation reaching it across all frequencies. The measurement is read many times per second to generate an interferogram. The interferogram is generated by recording the amount of radiation reaching the detector over time. This interferogram generated is called the background interferogram because it shows the energy passing through the components of the optical bench. A sample (material under investigation) is then placed in the path of the infrared beam. The frequencies of the infrared radiation that are absorbed and the strength of the absorptions are determined by the sample's chemical makeup. The resulting spectrum is called the sample interferogram.

The He-Ne laser produces a single frequency of red light that follows the same path of the infrared radiation. One of the functions of this laser is that it calibrates the spectrometer internally. The information contained in the background and the sample interferometer is recorded by the computer, where further processing takes place to produce the spectrum using OMNIC software version 7.3. The background and sample interferogram can also be called background single beam and sample single beam respectively. The computer (OMNIC) divides the sample single beam by the background single beam. The results show a transmission or absorption spectrum, which shows the change in intensity at each frequency that represent the absorption spectrum of the sample.

Measurements of Gases in Gas cells using the direct absorption method and the FT-IR spectrometer

Experiments were conducted to verify whether the direct absorption method would be able to detect gases placed in its path. In these experiments,

absorption measurements of gas cells containing an unknown concentration of benzyl alcohol was obtained from the Electrical Engineering Department at Princeton University and 100 ppm of 2-Methylphenol was purchased from Wavelength References Inc. These gases were contained in 38.1 cm x 12.7 cm gas cell for Benzyl alcohol and 5.1 cm x 2.5 cm gas cell for 2-Methylphenol. Figure 18 shows the schematic diagram for the direct absorption measurements for the gas cells. The collimated transmitted light from the QC laser (Intensity I_o) was measured with no gas placed in the path of the QC laser. A Lead Sulphide (PbS) Vigo detector was used to detect the collimated transmitted light after passing through the gas cells. The gas cells containing the two gases were simultaneously placed in the path of the QC laser beam and the transmitted intensity I recorded. A filter was placed in the set-up in order not to saturate the detector at the QC laser threshold current.
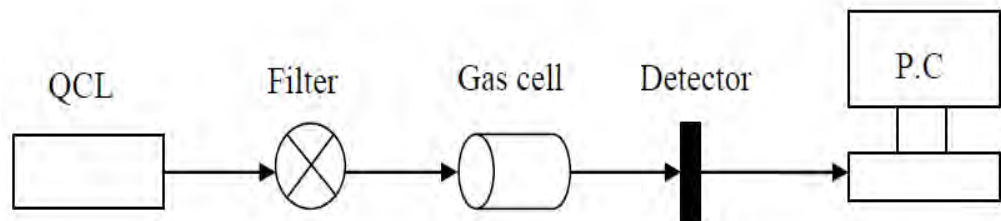
Figure 18: Schematic diagram for measuring the Absorbance of the gas cells using the direct absorption method

For the FT-IR spectrometer measurements, the background single beam was recorded by taking the infrared spectra without a sample (Benzyl alcohol and 2-Methylphenol) in the sample compartment. The two gas cells containing Benzyl alcohol and 2-Methylphenol were simultaneously placed in

the sample compartment and the sample single beam recorded. The absorbance of Benzyl alcohol and 2-Methylphenol was computed using the OMNIC software.

CHAPTER FOUR

RESULTS AND DISCUSSION

The first section of this chapter reports and discusses the results obtained from the Quantum Cascade Laser Open-Path System (QCLOPS) version 2 sensor and the Commercial humidity sensor. In the second section, results from the different wood samples received from Microlab Laboratory(an analytical chemistry company) is presented and discussed. The last section reports and discusses results obtained from the direct absorption of Benzyl alcohol and 2-methylphenol.

Results from the measurement of water vapour with the Commercial humidity sensor and QCLOPS version 2 sensor

The wavelength spectrum of the Quantum Cascade (QC) laser was measured with the Fourier Transform Infrared (FT-IR) Spectrometer and scans showed mode-hopping occurred in the spectrum of the QC laser. This implied that instead of a single pulse in the spectrum of the QC laser, there were two distinct pulses which showed two frequency peaks. This mode-hopping might be due to the drift in the temperature of the gain medium that shifted the wavelength of the maximum gain without the same shift occurring within the resonator mode frequencies. The shift in time of the absorption line of the QC laser happens as a result of self-heating effect (Webster et. al., 2001). Figure 19 illustrates the two scans of the QC laser controller which shows two

absorption peaks. The plot labelled Scan 1 had its absorption line at 1064 cm^{-1} but the second plot labelled scan 2 had its absorption line shifted to 1065 cm^{-1}. An enlarged scale is shown in the insert, which clearly shows the absorption peaks for water vapour which shifts its position from 1064 cm^{-1} to 1065 cm^{-1} for scan 1 and scan 2 respectively.
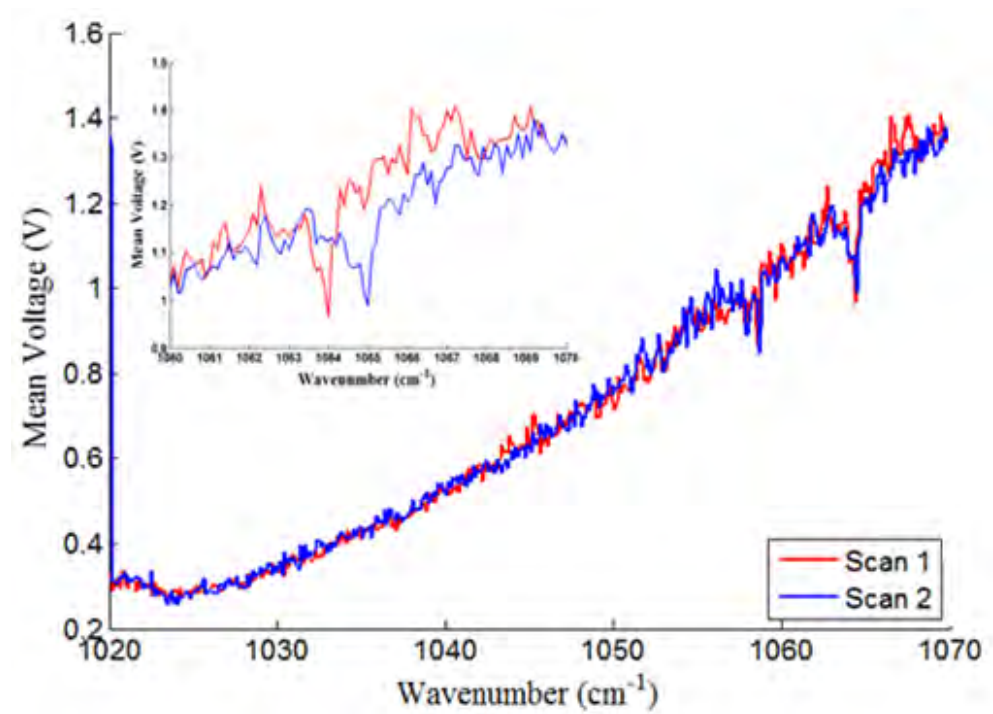
Figure 19: Mode-hopping in QC laser during two complete scans

Due to this, the results were standardised as the coefficient of variation, a dimensionless quantity, which is the ratio of the standard deviation of the measured values to the mean of the values. Figures 20a and 20b show the plot for the coefficient of variation of water vapour using the version 2 sensor and the mass concentration of water vapour using the humidity sensor from April 4, 2009 (6:00 PM - 12:00 PM.).
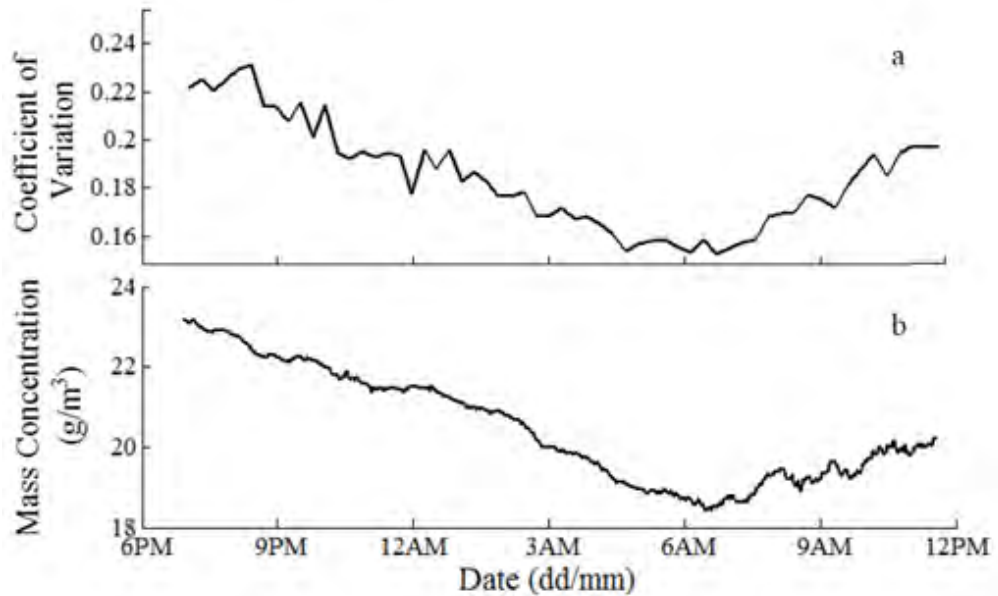
Figure 20: (a) Coefficient of variation against date from QCLOPS version 2 sensor from 6:00 PM to 12:00 PM. (b) Mass concentration (g/m^3) against date from the commercial humidity sensor from 6:00 PM to 12:00 PM

The two figures show a similar pattern as the mass concentration of the humidity sensor and the coefficient of variation for the version 2 sensor of water vapour decreases from around 6:40 PM down to about 6:30 AM where it attains its minimum value. There was a gradual increase in the quantity of water vapour in the atmosphere to about 11:30 PM in the evening. This behaviour about the two sensors with time may be as a result of the following discussions below:

At around 6:40 PM, the water vapour in the troposphere was high due to the high temperature during the day resulting in an increase in the rate of evaporation. As time elapsed from 6:40 PM to around 6:30 AM, the temperature began to decrease. The lower the temperature, the lower is the rate of evaporation and the higher the rate of condensation. This factor reduced the

mass concentration (coefficient of variation) of water vapour in the troposphere and hence the smaller the mass concentration.

At around 6:30 AM, the rate of evaporation had reached its minimum value where as the rate of condensation has also reached its maximum value. Hence the minimum mass concentration (coefficient of variation) was recorded at that time.

From that time, (i.e. 6:30 AM), the amount of radiation received by the earth's surface in this region starts increasing, resulting in the rise in day temperature. This rise in temperature leads to a corresponding rise in the rate of evaporation and the fall in the rate of condensation. Hence mass per unit volume of water vapour in the atmosphere also begins to rise resulting in the gradual increase of mass concentration (coefficient of variation) of water vapour from 6:30 AM to around 11:30 PM in the evening.

Figures 21 and 22show the mass concentration for the humidity sensor and the coefficient of variation for the version 2 sensor in the month of April, 2009. There was a break in data collection between the 8th and the 9th April 2009, due to power outages, and this affected both the version 2 sensor and the humidity sensor. The graphs for the mass concentration and the coefficient of variation for both the humidity sensor and the version 2 sensor respectively has been shown in Figures 20a and 20b. It can be seen from figures 21 and 22 that, few hours after the break the graphs look different.
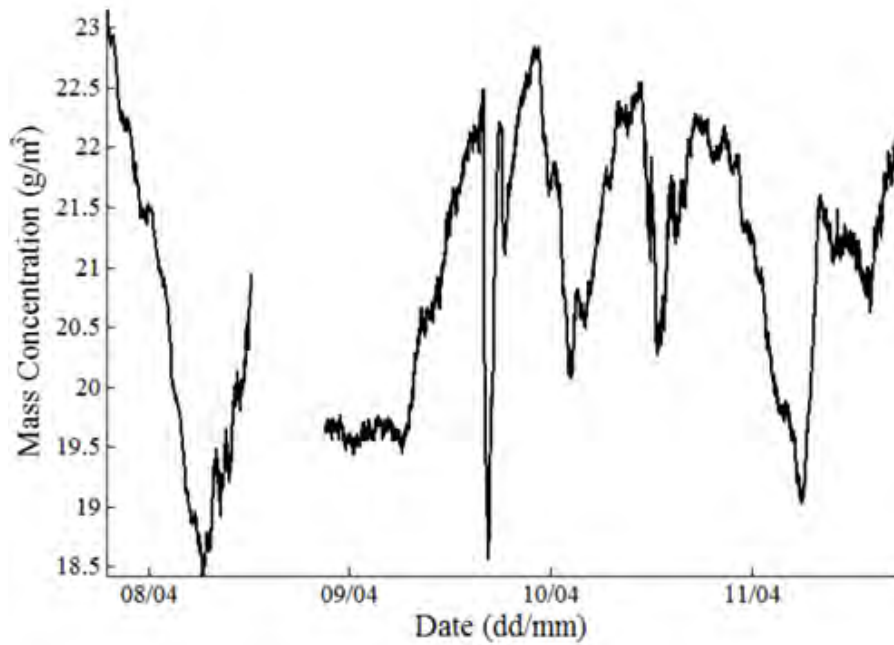
Figure 21: Mass concentration (g/m^3) against date for water vapour from the commercial humidity sensor from 8th to 11th April, 2009
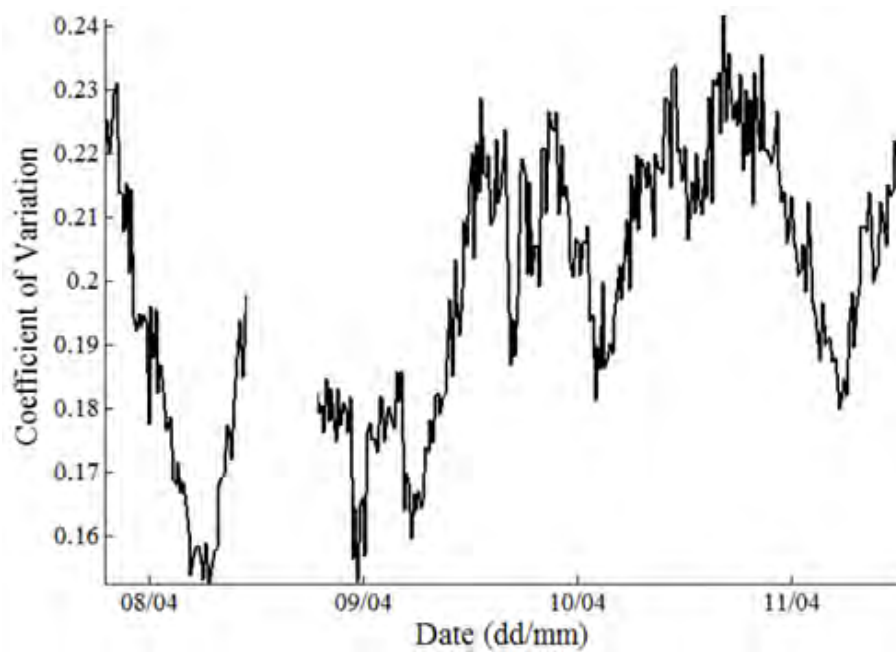
Figure 22: Coefficient of variation against date for water vapourfrom QCLOPS version 2 sensor from 8th to 11th April, 2009

It can be said that the humidity sensor responded well after the break while the version 2 sensor took a little while due to the long path of the QC laser. By mid-day the two systems returned to its normal operation where it was observed that there was a gradual increase in mass concentration (coefficient of variation) during the day to afternoon and it decreases again during the evening repeating the same pattern of increasing during the morning to late afternoon and decreasing in the evening all over again.
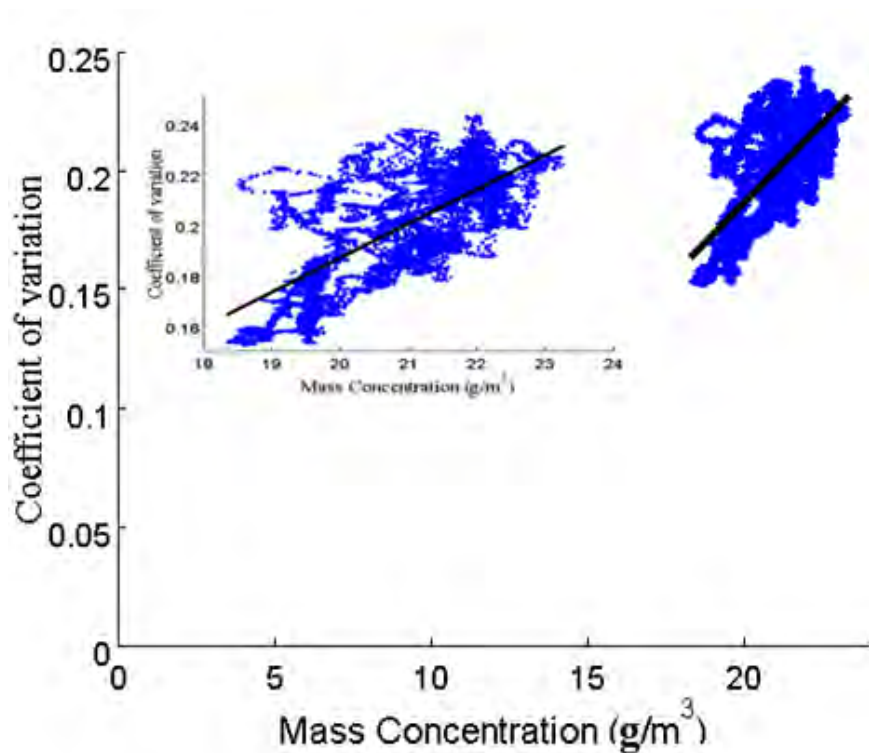
Figure 23: A plot of the coefficient of variation from the version 2 sensor against the mass concentration from the humidity sensor

The coefficient of variation from the version 2 sensor was compared with the mass concentration of the humidity sensor as shown in Figure 23. A linear relationship between the coefficient of variation and that of the mass concentration with a positive correlation coefficient of about 71.46 % was

obtained, implying a satisfactory agreement between the two measurements. The insert shows an enlarge scale of the coefficient of variation against the mass concentration showing a scatter plot of the amount of water vapour present.

Wood analysis

The gases were categorized into four main groups namely; volatile organic compounds (VOCs), semi-volatile organic compounds (SVOCs), metals and pesticides. When human beings are exposed to these gases, irrespective of their gas concentrations, can be dangerous to living things. The concentrations of the various gases found in the ten different wood species can be seen in the Appendix. The results presented here will dwell on the VOCs and SVOCs. Table 2 shows the VOCs of the ten different wood species and their respective gas concentrations in part per million (ppm). Figures 24-27 shows a bar graph of the gas concentrations of VOCs against the ten different wood species.

Results in table 2 shows Acetone, Acrolein, 2-Butanone and Benzene were in all the ten wood species but they all had varying gas concentrations in them. It can be seen from figure 24 that, the gas concentrations for acetone ranges between 65.2898 - 20.6254 ppm for all the ten wood species. Cocoa had a gas concentration higher than Esakoko. The high gas concentrations of acetone could be attributed to the fact that 97 % of acetone released to the atmosphere comes from natural sources, such as decomposing vegetation and forest fires (American Chemistry Council, 2003).

Table 2:Concentrations in ppm of VOCs of ten different wood species

Wood Species	Acetone (ppm)	Acrolein (ppm)	2-Butanone (ppm)	Benzene (ppm)
Kroma	65.2898	131.9121	20.6529	1.5723
Dwindwinaba	59.6538	71.6378	15.9787	0.8149
Esia	55.9627	86.6089	9.0606	1.0127
Yaya	50.6059	85.2311	15.1818	0.3982
Konkroma	49.1738	70.6290	14.1258	0.6876
Emire	42.9979	60.7029	12.5133	0.5924
Mango	35.1251	26.6099	14.1032	1.8760
Esakoko	30.5932	50.0133	9.0849	0.6225
Cocoa	32.3525	9.4528	9.1865	0.4939
Aborday	20.6254	25.5489	5.6554	0.6494
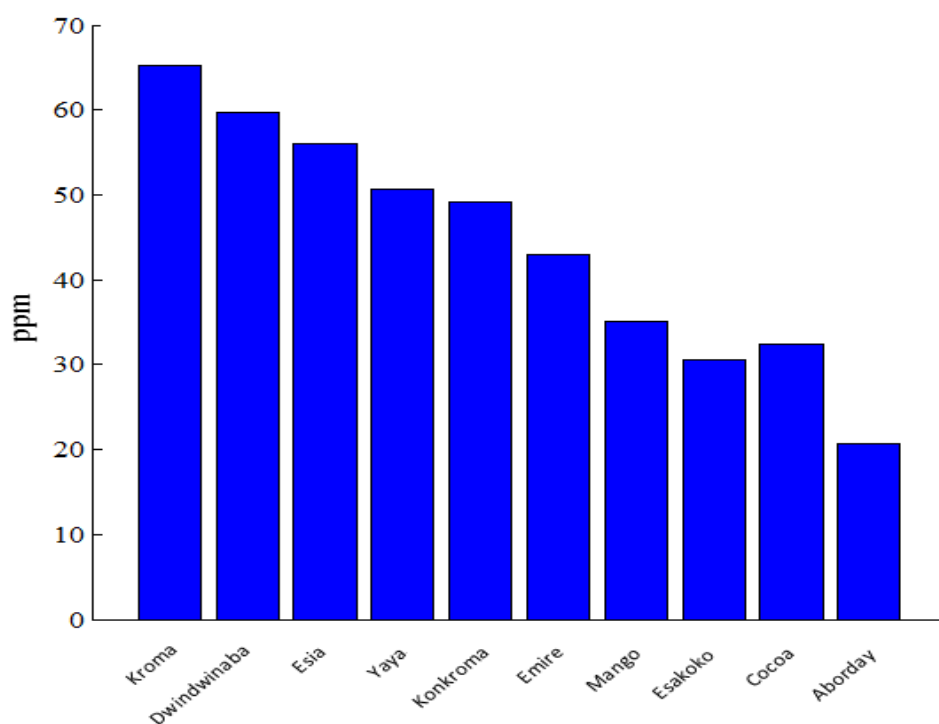
Figure 24: Acetonegas concentration from wood species
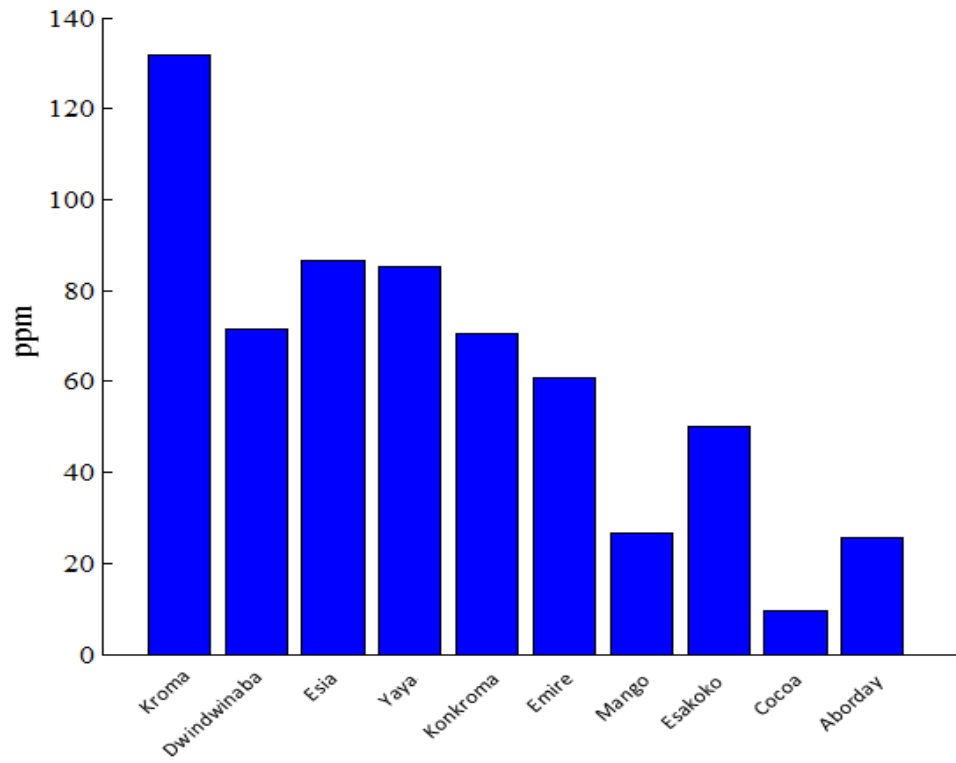
Figure 25: Acrolein gas concentration against wood species
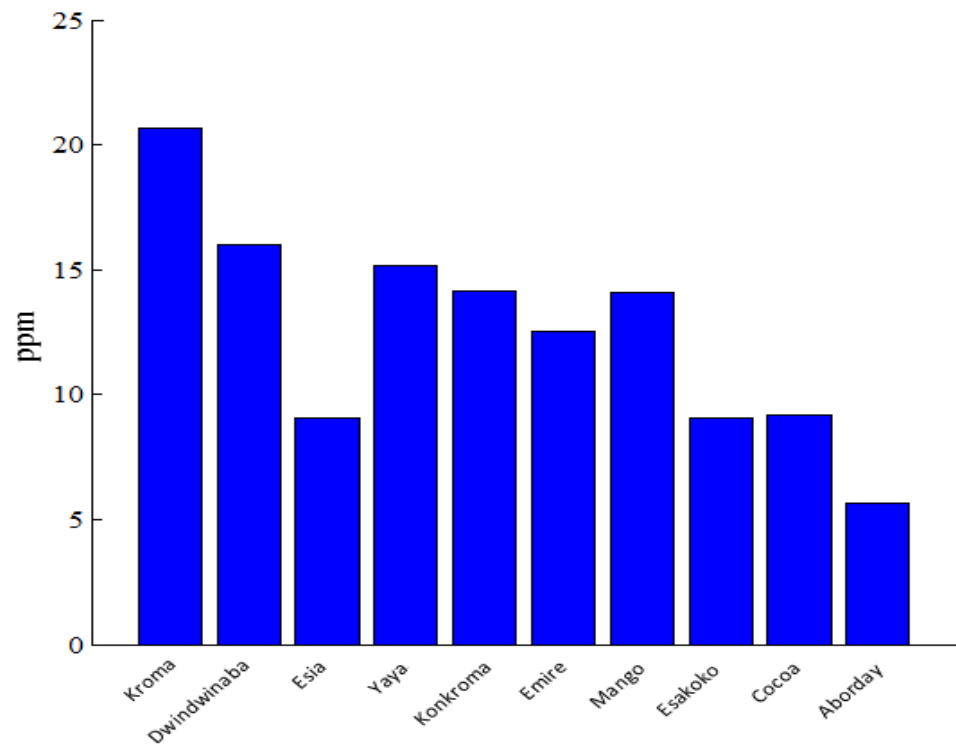
Figure 26: 2-Butanone concentration against wood species

Figures 25-27 shows a general trend of a decreasing gas concentration from Kroma to Aborday as seen from figure 24 with the exceptions of Dwindwinaba, Mango and Cocoa which had a relatively lower gas concentration for Acrolein. The same trend can be implied for 2- Butanone with the exception of Esia having a lower gas concentration and Benzene which had a relatively high gas concentration for Mango.
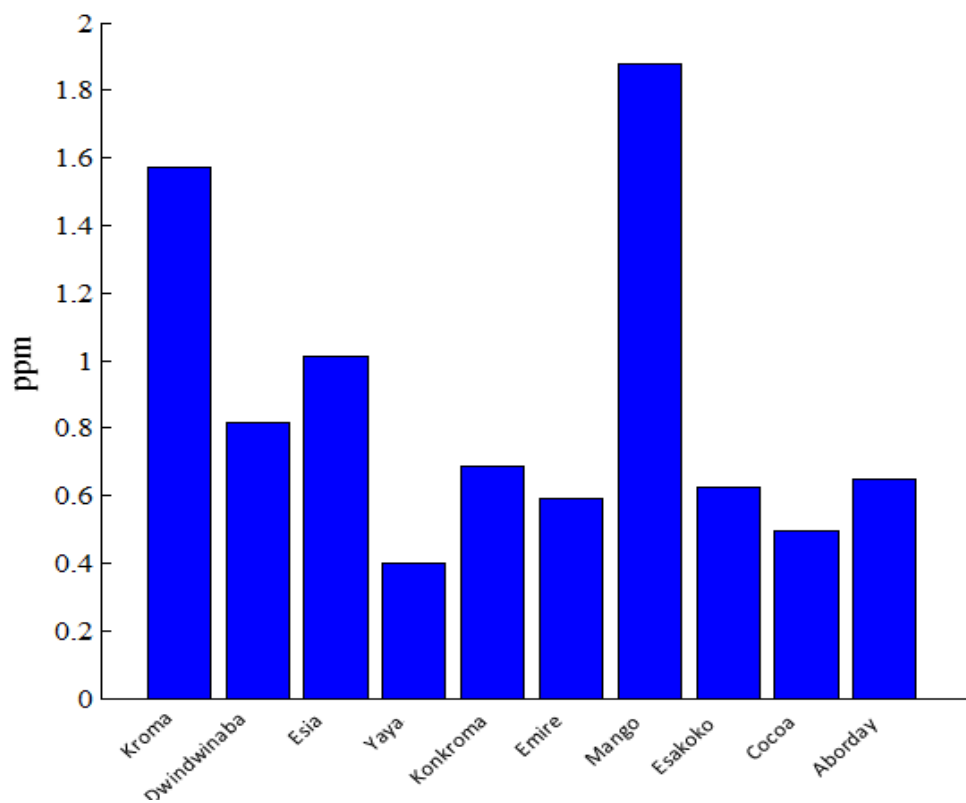
Figure 27: Benzene concentration against wood species

Table 3:Concentrations in ppm of SVOCs of ten different wood species.

Wood Species	Benzyl alcohol (ppm)	2-Methylphenol (ppm)
Esakoko	119.7127	5.3206
Mango	98.4566	3.8584
Esia	93.2712	4.1306
Konkroma	99.9467	3.6780
Kroma	74.6169	4.7702
Yaya	91.8897	2.3838
Dwindwinaba	33.2889	1.9441
Aborday	14.3713	0.9049
Cocoa	11.8493	0.6524
Emire	10.9159	0.2796

Some SVOCs emitted from the ten wood species are tabulated Table 3. The gases are 2-Methylphenol and Benzyl alcohol. Figure 28-29 shows a bar graph of these compounds with their corresponding wood species.
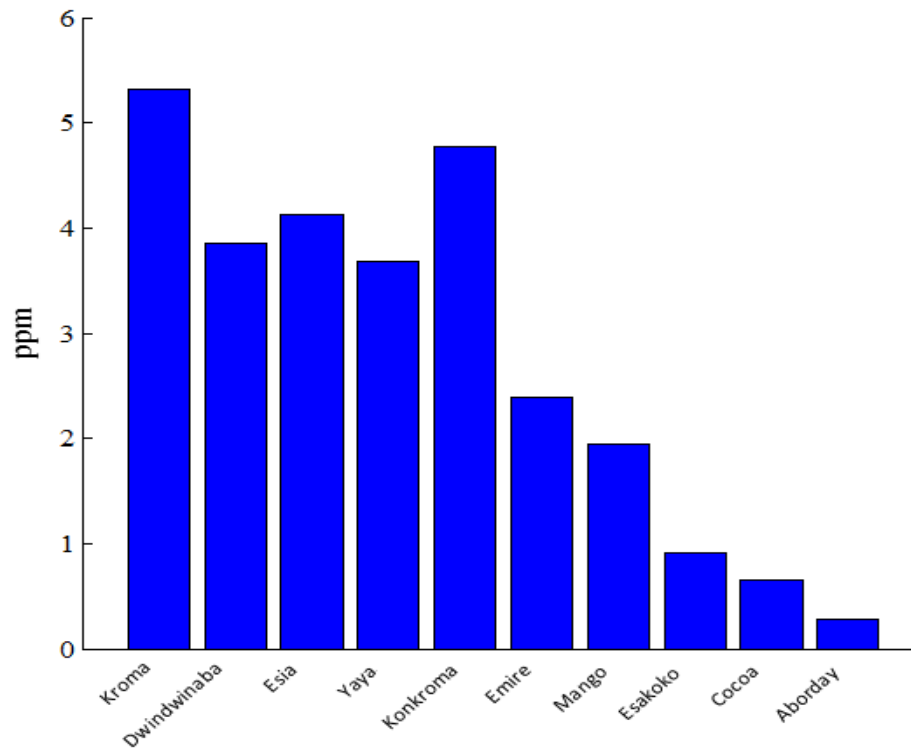
Figure 28: 2-Methylphenol concentration against wood species
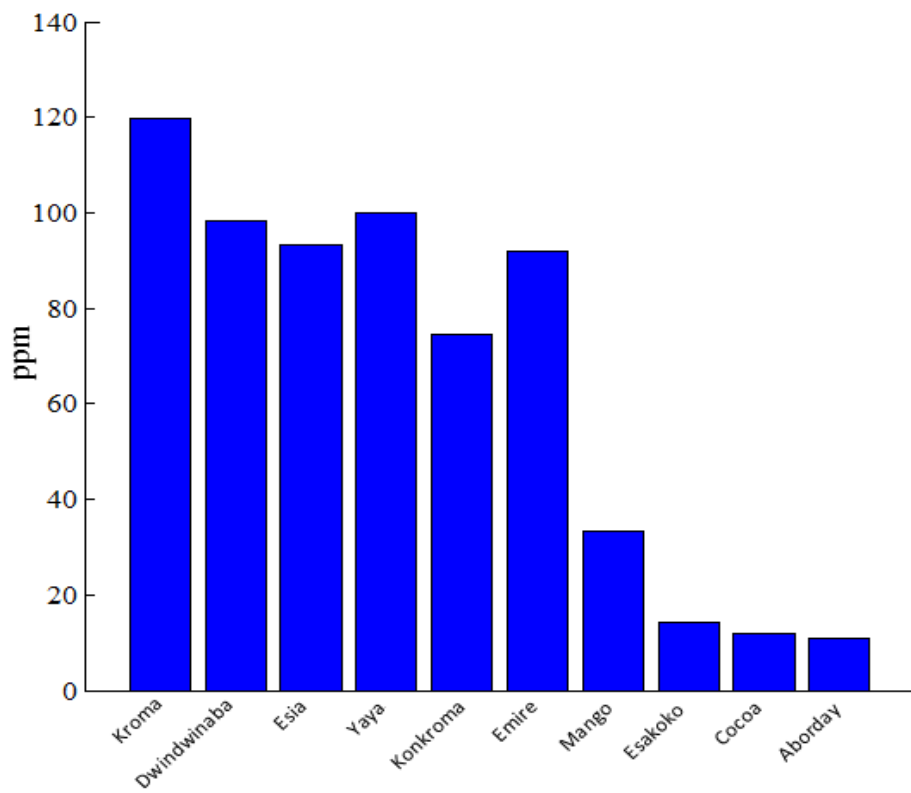
Figure 29: Benzyl alcohol concentration against wood species

Figures 28-29 show a similar trend of a decreasing gas concentration from Esakoko to Emire. Kroma had a high gas concentration for 2-Methylphenol but that of Benzyl alcohol reduced compared with the gas concentration for Esakoko, Mango, Esia, Konkroma and Yaya. Aborday, Cocoa and Emire maintained a low gas concentration for both 2-Methylphenol and Benzyl alcohol. Interestingly, the gas concentration for Mango in Benzene and 2-Methylphenol were really high as seen in figures 27 and 29 respectively. Figures 24-27 and 28-29 showed in order of decreasing gas concentration for the VOCs from Kroma to Aborday and for the SVOCs from Esakoko to Emire respectively.

It can therefore be concluded from figures 24-29 and from tables 2 and 3 that the wood species for Cocoa and Aborday should be used more by the fishmonger's to smoke their fish since the gases released by them both for the VOCs and SVOCs are relatively low as compared with the other wood species.

Absorbance Spectra from the FT-IR spectrometer and direct absorption method using the Uber Tuner

The absorbance of Benzyl alcohol and 2-Methylphenol were obtained from both the FT-IR spectrometer and direct absorption method. Figure 30 shows the normalized absorbance spectra for Benzyl alcohol, in the cell against wavenumber using the FT-IR spectrometer and the direct absorption method. The direct absorption method and the FT-IR spectrometer shows correct matching since Benzyl alcohol absorbs at a wavenumber of 1020, 1036 and 1080 cm^{-1}.
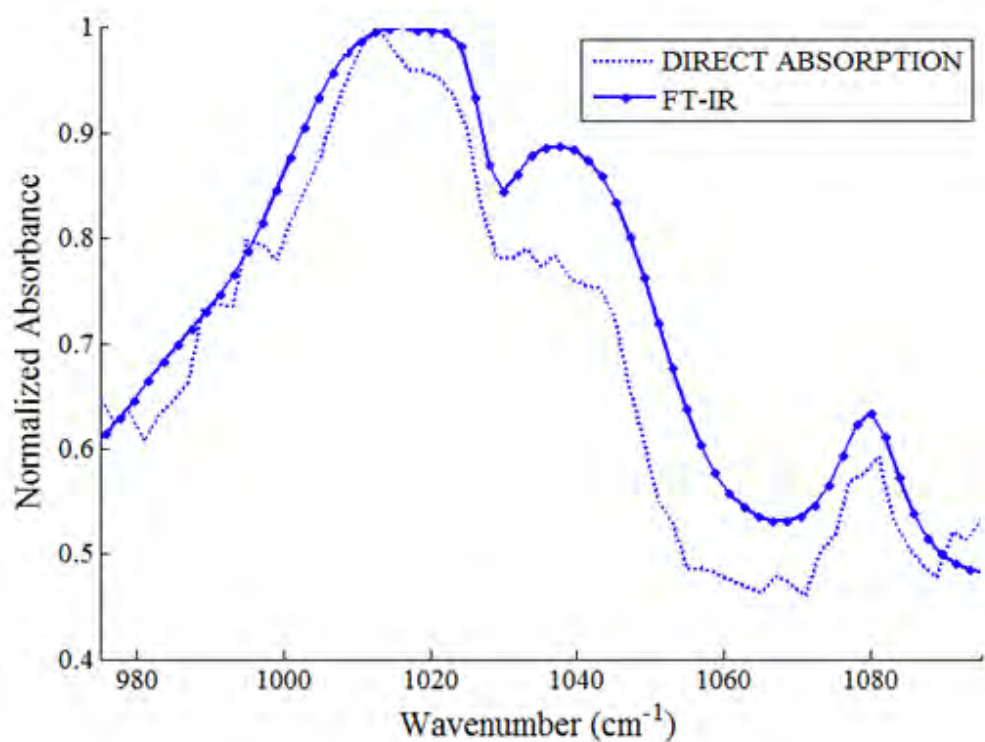
Figure 30: Normalized absorbance against wavenumber for Benzyl alcohol measured using the direct absorption method and FT-IR spectrometer

Moreover, figure 31 also illustrates the normalized absorbance spectra for 2-methylphenol, in a gas cell measured using the direct absorption method and the FT-IR spectrometer compared with the knowitall infrared spectra database. It can be seen from the graph that, the absorption peak for the direct absorption method for 2- Methylphenol around the wavenumber 1108 cm^{-1} shifted slightly to the right which could be as a result of the presence of water vapour when measurements were taken.The absorption wavenumber for 2-methylphenol occurred at 1108 and 1176 cm^{-1}.
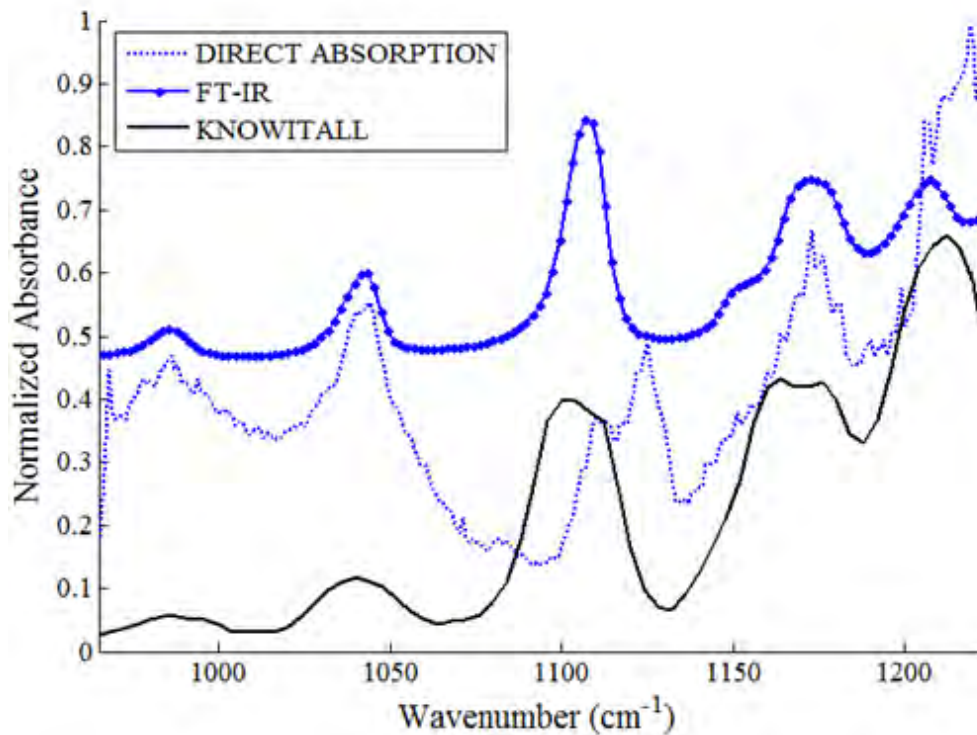
Figure 31: Normalized absorbance spectra for 2-Methylphenol measured using direct absorption method, FT-IR spectrometer and Knowitall Infrared database

The close agreements of Figures 30-31 show the capability of a future to be sensor built using a QC laser (Uber Tuner) in the wavenumber range of 965 to 1260 cm^{-1} be able to measure both Benzyl alcohol and 2-methylphenol in the field.

CHAPTER FIVE

CONCLUSION AND RECOMMENDATIONS

Conclusion

In this work, a Quantum Cascade Laser Open-Path System (QCLOPS) version 2 sensor had been set-up and used to measure water vapour concentration in the troposphere. There was mode-hopping in the QC laser spectrum resulting in the results being standardized as the coefficient of variation. A commercial humidity sensor was placed in close proximity to the version 2 sensor to also measure water vapour for comparison with version 2 sensor. Results obtained from the two sensors were very similar with water vapour decreasing from early evening to early morning (6:40 PM to 6: 30 AM) and rising steadily to the early afternoon (11:30 AM). The linear relationship established between the coefficient of variation of the version 2 sensor and the mass concentration of the humidity sensor showed a positive correlation of 71.46 %.

Analysis from ten different wood species used by fishmongers in a fishing community in Elmina studied had chemical compounds emitted when they were burnt. Several compounds were obtained from these wood species by Microlab Laboratories and they were grouped as metals, pesticides, volatile organic compounds (VOC) and semi-volatile organic compounds (SVOC). Four gases from VOC and two from SVOC were selected due to its high gas concentration. The gas concentration for the VOC ranged between 65.2898 -

20.6254, 131.9121 - 9.4528, 20.6529 - 5.6554, 1.8760 - 0.3982 ppm for Acetone, Acrolein, 2-Butanone and Benzene respectively and that for the SVOC ranged between 119.7127 - 10.9159 ppm for Benzyl alcohol and 5.3206 - 0.2796 ppm for 2-Methylphenol.

The infrared spectra of two target gases, 2-Methylphenol and Benzyl alcohol were measured using two different direct absorption method that is the QC laser (Uber Tuner) and a Fourier Transform Infrared (FT-IR) spectrometer showed or gave a satisfactory comparable results. In both cases, the systems showed an infrared absorption for Benzyl alcohol and 2-Methylphenol which occurred at 1020, 1036, 1080 and 1108, 1176 cm^{-1} respectively. Comparing the spectra with the knowitall infrared spectra database showed the capability of a future QC -Uber Tuner sensor incorporating the direct absorption method would be able to measure Benzyl alcohol and 2-Methylphenol in the field.

Recommendations

It is recommended that future work should be done to improve on the qualitative and quantitative measurements through the use of a QC laser with a narrower linewidth. Also, work could be done to investigate ways to avoid optical misalignments from changes in temperature in respect to the retroreflector. Further work could also be carried out on these harmful gases and the health risk associated with them.

REFERENCES

American Cancer Society.(2010). Benzene. Retrieved June 15, 2011, from http://www.cancer.org/cancer/cancercauses/othercarcinogens/inthewor kplace/benzene

American chemistry council. (2003), Acetone VCCEP submission.

Arthur, B. (2003). *Concepts of modern physics*. (6th ed.). Mcgraw Hill, New York.

Bahaa, B. E. A., &Malvin, T. C. (1991).*Fundamentals of Photonics*, Wiley Series in pure and applied optics: New York.

Baker, P. W. (1983). Atmospheric water vapour differential absorption measurements on vertical paths with CO2 lidar.*Appl.Opt*. **22(15)**, 2257- 2264.

Beck, M., Hofsteller, D., Aellen, T., Faist, J., Oesterle, U., Ilegems, M., Gini, E., &Melchoir, H. (2002).Continuous wave operation of a midinfrared semiconductor laser at room temperature, *Science*,**295**, 301-305.

Browell, E. V. (1983). Remote sensing of tropospheric gases and aerosols with an airborne DIAL system. In D. K. Killinger& A. Mooradian (Eds.), Optical and Laser Remote Sensing (pp. 138 – 147). *Springer – Verlag*, New York.

Cahen, C., Mergie, G., &Flamant P. (1982).Lidar monitoring of water vapour cycle in the troposphere.*J. Appl. Meteorol*. **21(10)**, 1506-1515.

Cooney, J. A. (1970). Remote measurements of atmospheric water vapour profiles using raman component of laser backscatter. J. Appl. Meteorol. **9(1)**, 182-184.

Cooney, J. A. (1971). Comparisons of water vapour profiles obtained by radio-soude and laser backscatter. **10(2)**, 301-308.

Curl, R. F., Capasso, F., Gmachl, C., Kosterev, A. A., McManus, B., Lewicki, R., Pusharsky, M., Wysocki, G., &Tittel, F. K. (2010). Quantum cascade lasers in chemical letters. *Chem. Phys. Lett.***487**, 1-18.

Devenson, J., Teissier, R., Cathabard, O., & Baranov, A. N. (2007).InAs/AlSb quantum cascade lasers emitting below 3 µm, *Appl. Phys. Lett.***90**, 111118-1

Faist, J., Gmachl, C., Capasso, F., Sirtor,i C., Sivco, D. L., Baillargeon, J. N. & Cho, A. Y.(1997). Distributed feedback quantum cascade lasers.*Appl. Phys. Lett*.,**70**, 2670.

Faist, J., Capasso, F., Sivco, D.L., Sirtori, C., Hutchinson A.L., & Cho, A.Y. (1994).Quantum cascade laser.*Science*, **264**, 553-556.

Filho, M. B., Da Silva, M. S., Schramm, D. U., Vargas, H., Millos, A., & Hess P. (2006).Ammonia detection by using quantum-cascade laser photoacousticspectroscopy.*App. Opt*. **45.**

Gmachl, C., Belyanin, A., Sivco, D. L., Peabody, M. L., Owschimikow, N., Sergent, A. M., Capasso, F., & A. Y. Cho. (2003). Optimized second-harmonic generation in quantum cascade lasers. *IEEE J. Quantum Electron*.**39**, 1345.

Gmachl, C., Capasso, F., Kohler, R., Trediccui, A., Hutchinson, L., Sivco, D. L., Baillargeon, J. N., & Cho A. Y. (2000). The sense ability of semiconductor lasers.IEEE, *Circuits and devices*.**20**, 10-17.

Gmachl, C., Capasso, F., Narimanov, E. E., Nockel, J. U., Stone, A. D., Faist, J., Sivco, D. L. & Cho A. Y. (1998). High-power directional emission from microlasers with chaotic resonators, *Science*.**280**, 1556-1564.

Gmachl, C., Sivco, D. L., Colombelli, R., Capasso, F. & Cho A. Y. (2002). Ultra-broadband Semiconductor laser, *Nature*, **415**, 883-887.

Hecht, E. (1998). *Optics*. (3rd ed.). Addison-Wesley.

Herriott, D. R., Kogelnik, H., &Kompfner, R. (1964). Off-axis paths in spherical mirror interferometers.*Appl. Opt*. **3**, 523-526.

Holthoff, E., Bender, J., Pellegrino, P., & Fisher A. (2010). Quantum Cascade Laser-Based Photoacoustic Spectroscopy for Trace Vapor Detection and Molecular Discrimination. *Sensor***10**, 1986-2002.

Jimenez, R., Taslakov, M., Simeonov, V., Calpini, B. Jeanneret, F., Hofstetter, D., Beck, M., Faist, J., & Bergh V. D. (2003). Ozone detection by differential absorption spectroscopy at ambient pressure with 9.6 μm pulsed quantum- cascade laser. *Appl. Phys B*.

Kazarinov, R. F., &Suris,R. A. (1971).Possibility of the amplification of electromagnetic waves in a semiconductor with a superlattice.*Fiz.Tekh.Poluprovodn*, **5**, 707-709.

Kohler, R., Tredicucci, A., Beltram, F., Beere, H. E., Linfield, E. H., Davies, A. G., Ritchie, D. A., Lotti, R. C., & Rossi, F. (2002). Terahertz Semiconductor heterostructure laser, *Nature*,**417**, 156.

Kosterev, A. A., Tittel, F. K., Kohler, R., Gmachl, C., Capasso, F., Sivco, D. Cho,L.,Wehe,A. Y.S., & Allen M. G. (2002). Thermoelectrically cooled quantum – cascade – laser – based sensor for the continuous monitoring of ambient atmospheric carbon monoxide. *App. Opt*. **41**.

Liu, Z., Wasserman, D., Howard, S., Hoffman, A., Gmachl, C., Wang, X., Tanbun-Ek, T., Cheng, L. &Choa F. (2006).Room-temperature continous-wave quantum-cascade lasers grown by MOCVD without lateral regrowth.*IEEE Photon. Technol. Lett*. **18**, 1347-1349.

Melfi, S. H., Lawrence, J. D., & McCormick, M. P. (1969).Observation of Raman scattering by water vapour in the atmosphere.*Appl. Phys. Lett*. **15(9)**, 295-297.

Michel, A.P., Liu, P. Q., Yeung, J. K., Corrigan, P., Baeck, M. L., Wang, Z., Day, T., Moshary, F., Gmachl, C. F., & Smith, J. A. (2010). Quantum cascade laser open-path system for remote sensing of trace gases in Beijing, China, *Opt. Eng*, **49**, 111125.

Murray, E. R. (1978). Remote measurement of gases using differential absorption lidar.*Opt. Eng*. **17(1)**, 30-38.

Murray, E. R., Hake, R. D., Van der Laan, J. E., & Hawley, J. G. (1976). Atmospheric water vapour measurements with a 10 micrometer DIAL system.*Appl. Phys. Lett*. **28(9)**, 542-543.

Owschimikow, N., Gmach,l C., Belyanin, A., Kocharovsky, V., Sivco, D. L., Colombelli, R., Capasso, F., & Cho, A. Y. (2003). Resonant second-order nonlinear optical processes in quantum cascade lasers, *Phys. Rev. Lett*.**90**, 043902-043904.

Pourny, J. C., Renaut, D., &Orszag, A. (1979).Raman-lidar humidity sounding of the atmosphereic boundary layer.*Appl. Opt*. **11(7)**, 1605-1610.

Roberts, J. S., Green, R. P., Wilson, L. R., Zibik, E. A., Revin, D. G., Cockburn, J. W. &Airey, R. J. (2003). Quantum cascade lasers grown by metal organic vapor phase epitaxy, *Appl. Phys. Lett*.,**82**, 4221.

Roller, C., Kosterev, A. A., Tittel, F. K., Gmachl, C., Sivco, D. L. (2003).Carbonyl sulphide detection with thermoelectrically cooled midinfrared quantum cascade laser.*Opt.Lett*. **28**,2052-2054.

Rothe, K. W. (1980). Monitoring of various atmospheric constituents using a cw chemical hydrogen/deuterium laser and a pulsed carbon dioxide laser.*Radio Electron Eng*. **50(11/12)**, 567-574.

Schafer, F. P. &Drexhage, K. H. (1977).*Dye lasers*. (2nded.). Springer-Verlag, New York.

Schotland, R. M. (1975). Upper bound estimate on the resonance cross section for water vapour at 694.38 nm.*J. Appl. Meteorol*. **14(12)**, 1615-1617**.**

Siegman, A. E. (1986). *Lasers*.Printed in United States of America.

Sigrist, M. W. (Ed). (1994). *Air Monitoring by Spectroscopic Techniques*.**127**, John Wiley and Sons, Inc.

Sirtori, C., Kruck, P., Barbieri, S., Collot, P., Nagle, J., Beck, M., Faist, J., &Oesterle U. (1998).GaAs/Al_xGa_{1-x}As quantum cascade lasers, *Appl. Phys. Lett*.,**73**, 3486

Stuart, B. (2004). Infrared Spectroscopy: *Fundamentals and Applications*. John Wiley & Sons, Incoporated, New Jersey.

Svelto, O. (1998). *Principles of Lasers*. (4thed.). Plenum Press, New York.

Taslakov, M., Simeonov, V., Froidevaux, M., & Bergh V. D. (2006).Open-path ozone detection by quantum-cascade laser.*Appl. Phys. B*. **82**, 501-506.

The free dictionary.(n.d.). Hyperfine Structure. Retrieved June 22, 2011 from http://encyclopedia2.thefreedictionary.com/Hyperfine+structure

The free dictionary.(n.d.). Molecular structure and spectra. Retrieved June 22, 2011

from http://encyclopedia2.thefreedictionary.com/Molecular+structure+and+spectra

The free dictionary.(n.d.). Nuclear moments. Retrieved June 22, 2011 from http://encyclopedia2.thefreedictionary.com/Nuclear+moments

U. S. Environmental Protection Agency. (2008). Retrieved June 15, 2011, from http://www.epa.gov/ttnatw01/hlthef/benzene.html

United States Department of Labor.(n.d.).Benzene. Retrieved June 15, 2011, from http://www.osha.gov/SLTC/benzene/

Verdeyen, J. T. (1995). Laser Electronics, Prentice Hall Series in solid state physical electronics. (3 rd ed.). Prentice Hall.

Water Vapour Confirmed as Major Player in Climate Change. (n.d). Retrieved May 26, 2011, from http://www.nasa.gov/topics/earth/features/vapor_warming.html

Webster, C.R., Flesh, G. J., Scott, D. C., Swanson, J. E., May, R. D., Woodward, W. S., Gmachl, C., Capasso, F., Sivco, D. L., Baillargeon, J. N., Hutchinson, A. L., Cho A. Y. (2001): Quantum cascade laser measurements of stratospheric methane and nitrous oxide.*Appl. Opt*. **40**, 321-326.

White, J. U. (1942). Long Optical Paths of Large Aperture. *J. Opt. Soc. Am*. **32(5)**, 285-288.

Williams, B. S., Callebaut H., Kumar, S., & Hu, Q. (2003). 3.4-THz quantum cascade laser based on longitudinal-optical-phonon scattering for depopulation.*Appl. Phys. Lett*. **82**, 1015.

Yariv, A., &Yeh, P., (2007). *Photonics: Optical electronics in modern communications*. (6th ed.). Oxford University Press, New York.

Zuel, V. V., Zuel ,V. E., Makushkin, Y. S., Marichev, V. N., &Mitsel, A. A. (1983). Laser sounding of atmospheric humidity: experiment. *Appl. Opt*. **22(23)**, 3742 – 3746.

APPENDIX

The concentrations in part per billion (ppb) were first gotten from the convection below:

Microgram per Kilogram (ppb) = µg/Kg

For example, the average mass for the log of Esakokoo was 0.002506 Kg. When this mass was burnt, an amount of 246.6667 µg/sample of Benzyl alcohol was detected. Therefore, with the convection above, the concentrations in ppb was gotten by dividing the mass of Benzyl alcohol with the mass of Esakoko. It was then divided by 1000 to get the concentrations inppm.

VOLATILE ORGANIC COMPOUNDS (VOCs)

Wood Species	Acetone (ppm)	Acrolein (ppm)	Benzene (ppm)
Mango	35.125533868	26.610252930	1.876022832
Yaya	50.605939539	85.231056066	0.398188840
Esia	55.955235811	86.597388756	1.012523315
Esakoko	30.593242884	50.013301410	0.622505986
Konkroma	49.174429297	70.629939098	0.687642426
Dwindwinaba	59.654589275	71.638770157	0.814924300
Aborday	20.625415835	25.548902196	0.649367931
Emire	42.997870075	60.702875399	0.592385517
Cocoa	32.352118864	9.452676705	0.493935642
Kroma	65.288936856	131.910300995	1.572264194

Wood Species	2-Butanone (ppm)	Carbon Disulfide (ppm)	Chloromethane (ppm)
Mango	14.103434053	0.971274232	1.390385716
Yaya	15.181781862	0.258356639	1.345052604

Esia	9.059419131	0.159872102	17.319477751
Esakoko	9.084862995	0.505453578	1.729183293
Konkroma	14.125987820	0.127933475	16.391476432
Dwindwinaba	15.978907842	0.306262400	51.132505093
Aborday	5.655355955	1.064537591	16.540252828
Emire	12.513312034	0.505857295	53.248136315
Cocoa	9.186404122	1.025149445	2.849116641
Kroma	20.652622883	0.559619459	17.188311948

Wood Species	Methylene chloride (ppm)	Toluene (ppm)	m,p-Xylene (ppm)
Mango	1.130935750	1.663140808	0.292712782
Yaya	1.398322014	0.932214676	---------------
Esia	1.385558220	1.598721023	---------------
Esakoko	1.503059324	0.851290237	0.121042831
Konkroma	0.906195445	1.479230800	0.265195432
Dwindwinaba	1.118523549	1.422122798	0.133157565
Aborday	1.197604790	0.838323353	---------------
Emire	0.998402556	0.692225772	---------------
Cocoa	0.918640412	1.144972108	---------------
Kroma	0.985996189	2.118559380	0.274480020

Wood Species	Ethylbenzene (ppm)	Styrene (ppm)	2-Hexanone (ppm)
Mango	0.154339467	0.172966644	---------------
Yaya	--------------	--------------	--------------

Esia	---------------	---------------	--------------
Esakoko	---------------	---------------	--------------
Konkroma	0.149255720	0.066632018	0.333160090
Dwindwinaba	0.073236661	---------------	---------------
Aborday	---------------	---------------	--------------
Emire	---------------	---------------	--------------
Cocoa	---------------	---------------	--------------
Kroma	0.153229138	0.054629519	---------------

Wood Species	4-Methyl-2-Pentanone (ppm)	1,1,1-Trichloroethane (ppm)	Surr:4-Bromofluorobenzene
Mango	0.172966644	---------------	---------------
Yaya	---------------	---------------	--------------
Esia	---------------	---------------	--------------
Esakoko	---------------	---------------	--------------
Konkroma	---------------	---------------	--------------
Dwindwinaba	---------------	---------------	--------------
Aborday	---------------	---------------	--------------
Emire	---------------	0.439297125	---------------
Cocoa	---------------	---------------	--------------
Kroma	---------------	---------------	40.505789397

SEMI-VOLATILE ORGANIC COMPOUNDS (SVOCs)

Wood Species	2-Methylphenol (ppm)	Benzyl alcohol (ppm)	Bis(2-ethylhexyl)phthalate (ppm)

Mango	3.858486675	98.457935843	2.035684349
Yaya	2.383806099	91.889732321	3.622319883
Esia	4.130029310	93.258726352	1.025845990
Esakoko	5.320563980	119.712689545	---------------
Konkroma	3.678087395	99.948027026	3.011767214
Dwindwinaba	1.944100454	33.289391337	1.105207792
Aborday	0.904856953	14.371257485	0.359281437
Emire	0.279552716	10.915867945	1.331203408
Cocoa	0.652367829	11.849129954	0.426036133
Kroma	4.770089672	74.615927836	9.073829796

Wood Species	2,4-Dimethylphenol (ppm)	Diethyl phthalate (ppm)	1,4-Dichlorobenzene (ppm)

Wood Species			
Mango	1.463563911	1.915938211	2.501363775
Yaya	---------------	0.905579971	0.838993208
Esia	1.052491340	---------------	---------------
Esakoko	2.553870710	---------------	---------------
Konkroma	---------------	1.292661150	---------------
Dwindwinaa	0.133157565	0.945418714	---------------
Aborday	0.425815037	---------------	---------------
Emire	---------------	---------------	0.133120341
Cocoa	0.133136292	---------------	---------------
Kroma	2.518287564	---------------	---------------

Wood Species	Dibenzofuran (ppm)	Phenol (ppm)	Butyl benzyl phthalate (ppm)
Mango	---------------	4.789845527	---------------
Yaya	---------------	---------------	---------------
Esia	---------------	---------------	---------------
Esakoko	---------------	---------------	---------------
Konkroma	---------------	---------------	---------------
Dwindwinaba	---------------	---------------	---------------
Aborday	0.328675981	---------------	---------------
Emire	---------------	---------------	---------------
Cocoa	---------------	---------------	---------------
Kroma	0.826104915	---------------	0.946023371

TOTAL METALS

Wood Species	Chromium	Mercury (ppm)	Zinc (ppm)

	(ppm)		
Mango	0.000287391	0.000009447	0.000465679
Yaya	0.000195765	0.000008923	0.001970968
Esia	0.000301092	0.000008793	0.001891820
Esakoko	0.000155626	0.000008114	0.001968609
Konkroma	0.000333160	0.000009595	0.000453098
Dwindwinaba	0.000153131	0.000008922	0.001318260
Aborday	0.000250166	0.000012508	0.000971391
Emire	0.000166400	0.000009585	0.000332801
Cocoa	0.000116095	0.000009586	0.000332841
Kroma	0.000253161	0.000008661	0.001412373

Wood Species	Lead (ppm)	Cadmium (ppm)	Copper (ppm)
Mango	0.000011975	0.000002262	---------------
Yaya	---------------	---------------	0.000133174
Esia	---------------	---------------	0.000243805
Esakoko	0.000010109	0.000004123	0.000085129
Konkroma	0.000014659	---------------	0.000133264
Dwindwinaba	0.000022637	0.000005726	---------------
Aborday	0.000065203	0.000011577	---------------
Emire	0.000012513	0.000002929	---------------
Cocoa	0.000012515	0.000002929	---------------
Kroma	0.000014657	0.000005330	0.000146567

Wood Species	Nickel (ppm)	Selenium (ppm)	Silver (ppm)

Wood Species			
Mango	---------------	0.000078500	0.000015035
Yaya	---------------	0.000017313	---------------
Esia	---------------	---------------	0.000004929
Esakoko	0.000106411	0.000087789	0.000012104
Konkroma	---------------	---------------	0.000019057
Dwindwinaba	0.000008922	0.000029295	---------------
Aborday	0.000023686	---------------	---------------
Emire	0.000039936	---------------	---------------
Cocoa	0.000039941	---------------	---------------
Kroma	0.000008927	---------------	---------------

Wood Species	Thallium (ppm)	Antimony (ppm)
Mango	---------------	---------------
Yaya	---------------	---------------
Esia	---------------	---------------
Esakoko	---------------	0.000017292
Konkroma	---------------	---------------
Dwindwinaba	0.000025300	---------------
Aborday	---------------	---------------
Emire	---------------	---------------
Cocoa	---------------	---------------
Kroma	---------------	---------------